UCRL-19107

c. 2

RECEIVED
LAWRENCE
RADIATION LABORATORY
JAN 28 1970
LIBRARY AND
DOCUMENTS SECTION

STRAIN HARDENING OF LONG RANGE ORDERED SILVER MAGNESIUM SINGLE CRYSTAL

Mohamed Osama Aboel Fotoh
(Ph.D. Thesis)

December 1969

AEC Contract No. W-7405-eng-48

TWO-WEEK LOAN COPY

This is a Library Circulating Copy which may be borrowed for two weeks. For a personal retention copy, call Tech. Info. Division, Ext. 5545

UCRL-19107

LAWRENCE RADIATION LABORATORY
UNIVERSITY of CALIFORNIA BERKELEY

DISCLAIMER

This document was prepared as an account of work sponsored by the United States Government. While this document is believed to contain correct information, neither the United States Government nor any agency thereof, nor the Regents of the University of California, nor any of their employees, makes any warranty, express or implied, or assumes any legal responsibility for the accuracy, completeness, or usefulness of any information, apparatus, product, or process disclosed, or represents that its use would not infringe privately owned rights. Reference herein to any specific commercial product, process, or service by its trade name, trademark, manufacturer, or otherwise, does not necessarily constitute or imply its endorsement, recommendation, or favoring by the United States Government or any agency thereof, or the Regents of the University of California. The views and opinions of authors expressed herein do not necessarily state or reflect those of the United States Government or any agency thereof or the Regents of the University of California.

TABLE OF CONTENTS

ABSTRACT

I. INTRODUCTION ---------- 1

II. EXPERIMENTAL PROCEDURE ---------- 10

III. EXPERIMENTAL RESULTS ---------- 13

A. Effect of Orientation and Temperature on the Flow Stress --- 14

B. Effect of Orientation and Temperature on the Slip System --- 19

C. Effect of Orientation and Temperature on the Strain Hardening ---------- 21

IV. DISCUSSION OF RESULTS ---------- 24

V. SUMMARY ---------- 38

ACKNOWLEDGEMENTS ---------- 39

REFERENCES ---------- 40

FIGURES ---------- 42

STRAIN HARDENING OF LONG RANGE ORDERED SILVER MAGNESIUM SINGLE CRYSTAL

Mohamed Osama Aboel Fotoh

Inorganic Materials Research Division, Lawrence Radiation Laboratory
Department of Materials Science and Engineering, College of Engineering
University of California, Berkeley, California

ABSTRACT

The deformation behavior of single crystals of AgMg intermetallic compound (CsCl type structure) of various orientations in the standard stereographic triangle was investigated in tension over the range from 20°K to 300°K and in compression at 237.5°K. The plastic behavior shows asymmetry in both the critical resolved shear stress for slip on the{112} planes and in the strain hardening.

Crystals oriented near the [001] direction deform in tension by slip in the $[\bar{1}11]$ direction and on well defined crystallographic $(1\bar{1}2)$ planes in the range from 20°K to 300°K, while those oriented near the $[\bar{1}11]$-[011] boundary deform in tension by slip on a system of the form {hk0} ⟨001⟩ in the range from 50°K to 300°K. Crystals oriented near the $[\bar{1}11]$-[011] boundary deform in compression by slip on the $(\bar{2}11)$[111] system.

The tensile flow stress of crystals oriented near the [001] direction is found to depend strongly on temperature in the range from 20°K to ~ 250°K, while the tensile flow stress of crystals in orientations near the $[\bar{1}11]$-[011] boundary is relatively independent of temperature in the range from 50°K to 300°K.

Crystal oriented for ⟨111⟩ slip exhibit classical single crystal stress-strain curves having a region of easy glide followed by a linear

region of relatively low rates of strain-hardening. In contrast, crystals oriented for ⟨001⟩ slip yield parabolic stress-strain curves with high rates of strain-hardening.

The high strain-hardening rates exhibited by AgMg single crystals is qualitatively explained in terms of a model based on the recombination of the dissociated partials, a/2[111] and a/2[111], of the superdislocation and the subsequent dissociation of the recombined segment of a[111] screw dislocation into a[110] and a[001] dislocations. The relatively low rates of strain hardening are due mainly to elastic and short-range interactions with the intersection dislocations.

The strain hardening behavior of AgMg single crystals does not appear to be due to Vidoz-Brown mechanism of forming athermal barriers to the motion of superdislocations by the creation of tubes of antiphase boundary as a result of jogs formed by the intersection with mobile forest superdislocations.

I. INTRODUCTION

The operative glide modes, the mechanisms of slip and the work hardening characteristics of long-range ordered alloys and intermetallic compounds that crystallize in the B_2 lattice (CsCl type structure) are interesting not only from a practical viewpoint but equally from their theoretical implications. Whereas some B_2 alloys slip along the ⟨111⟩ vector, in a manner similar to that for bcc metals and their randon solid-solution alloys, other slip along the ⟨001⟩ vector somewhat typical for ionic materials. The origin of these differences in terms of anti-phase boundary (APB) energies, γ_A, was first suggested by Rachinger and Cottrell.[1] In metallic systems of B_2 crystals the superdislocation a[111], where a is the lattice constant, will dissociate according to

$$a[111] \rightarrow a/2[111] + a/2[111] \qquad (1)$$

with a change in energy per unit length of about $-3/4 \frac{Ga^2}{(1-\nu)}$, where G is the shear modulus of elasticity and ν is Poisson's ratio for edge dislocations and zero for screw dislocations. The equilibrium separation d, of the two halves of the dissociated superdislocation, obtained when their mutual repulsion force is equal to the attractive force due to the antiphase-boundary (APB) is

$$\frac{3a^2G}{8\pi\,(1-\nu)\,d} - \gamma_A = 0 \qquad (2)$$

For γ_A approaching zero, the separation of the two halves of the super-dislocation is so great and their interaction so small that each a/2[111] dislocation reacts substantially independently of the other. In this event the deformation characteristic of B_2 lattices should approach those of bcc metals and their random solid-solution alloys. A crude estimate

of the values $0 \leq \gamma_A \leq \gamma_{A_1}$ over which this is expected to happen might be given by selecting $d = d_1 \simeq 100\ a/2[111] = 50\sqrt{3}a$, hence

$$\gamma_{A_1} \simeq \frac{\sqrt{3}\ aG}{400\pi(1-\nu)} \tag{3}$$

A typical examples of B_2 intermetallic compounds which have a very small values of, γ_A, is the B_2 compound CuZn. Slip in β-CuZn was reported to occur on a system of the form {110} ⟨111⟩[1-5] which is typical slip system of bcc metals and their random solid-solution alloys.

For extremely higher values of γ_A, the separation of the two halves of the superdislocation will be negligible. An estimate of the required critical value γ_{A_2} when this occurs can be obtained by placing $d = d_2 \simeq a/2[111] = a/2\sqrt{3}$ hence

$$\gamma_{A_2} \gtrsim \frac{\sqrt{3}\ aG}{4\pi(1-\nu)} \tag{4}$$

Under these conditions the superdislocation can dissociate without change in energy according to

$$a[111] \rightarrow a[100] + a[010] + a[001] \tag{5}$$

Each dissociated part of the superdislocation is the smallest identity distance in the B_2 lattice and since their Burgers vectors are mutually orthogonal, each split dislocation will move independently of the others. In this case the deformation characteristics are expected to approach those obtained in CsCl type ionic crystals which have extremely high values of γ_A arising from coulombic repulsions of ions of the same sign across the antiphase-boundary (APB). A typical examples of B_2 intermetallic compounds which have a very high values of, γ_A, is the B_2 compound NiAl. Slip in β'-phase NiAl was reported to occur on system of the form {110} ⟨001⟩[5-7] which is typical slip system of CsCl type ionic crystals.

The most interesting examples of B_2 intermetallic compounds and long-range ordered alloys occur for those examples where

$$\frac{\sqrt{3}a\ G}{400\pi(1-\nu)} \leq \gamma \leq \frac{\sqrt{3}a\ G}{4\pi(1-\nu)}.$$

In this range of antiphase-boundary energies the motion of the two dissociated halves, a/2[111] and a/2[111], of the superdislocation are coupled through the intervening antiphase-boundary (APB). Since the two halves of the superdislocation are separated they cannot recombine and dissociate in accord with Eq. 5 without the expenditure of the recombination energy. In general they will be confined to glide on their slip planes giving deformation characteristics typical of ordered B_2 alloys.

The preceeding analyses on operative slip vectors for B_2 ordered phases and intermetallic compounds were based on the assumption of elastic isotropy and on physical intuition regarding the limits of ranges of behavior in establishing γ_{A_1} and γ_{A_2}. Consequently they serve as a qualitative guides to the actual cases rather than a quantitative evaluation of the situations. As will be shown later, the previously described theory for predicting operative slip vectors in alloys that crystallize on the B_2 lattice is rather good. In contrast, however no equally satisfactory method has been developed for predicting their glide planes. Glide planes must obviously be in the zone of the Burgers vector. On a purely empirical basis they are known to be low-index planes which have the greatest interplanar spacings. Undoubtedly the operative slip planes are those on which the Peierls stress is the lowest but the theoretical approaches for determining Peierls stresses, however are not yet sufficiently well developed to provide reliable predictions.

In bcc metals and many of their solid-solution alloys glide takes place on planes of the forms $\{\bar{1}01\}$ and $\{\bar{1}\bar{1}2\}$. Recently carefully gathered evidence strongly suggests that the previously reported $\{\bar{1}\bar{2}3\}$ $\langle 111\rangle$ slip mode arises from intimate $\{\bar{1}01\}$ and $\{\bar{1}\bar{1}2\}$ cross-slip. Consequently the

$\{\bar{1}01\}$ and $\{\bar{1}\bar{1}2\}$ glide planes are expected to be operative for B_2 alloys where $0 \leq \gamma \leq \gamma_{A_1}$

Slip in B_2 alloys for which $\gamma_{A_1} \leq \gamma_A \leq \gamma_{A_2}$ should take place by the coupled motion of the two a/2[111] halves of the superdislocation. Cross slip should be easier from planes of higher to ones of lower antiphase-boundary (APB) energies. On (hkl) planes of B_2 alloys according to nearest neighbor interaction energies, the antiphase-boundary energy (APB) energy is given by[8]

$$\gamma_A = \frac{-4h\epsilon\, n^2}{a^2\sqrt{h^2+k^2+\ell^2}} \quad \text{for } h \geq k + \ell \qquad (6)$$

where n is the degree of order for long-range ordered alloys and unity for stoichiometric intermetallic compounds and ϵ is the bond ordering energy, namely

$$\epsilon = \epsilon_{AB} - 1/2\,(\epsilon_{AA} + \epsilon_{BB}) \qquad (7)$$

Since as shown by Eq. 6, γ_A is least for the lowest index planes, it is expected that the preferred planes of slip will be of the form $\{\bar{1}01\}$ unless the Peierls stress is lower on other planes e.g. $\{\bar{1}\bar{1}2\}$. Minor deviations from such predictions, however, might be due to inaccuracies introduced into the analysis by simplifying assumptions of (a) calculating γ_A on the basis of nearest neighbor interactions and (b) estimating the separation of the halves of the a[111] superdislocation in terms of isotropic elasticity.

The criteria that the operative slip planes are those of low index lying in the zone of the shortest translation vector of the lattice apply to ionic as well as metallic crystals. For ionic crystals, however, the additional restriction that slip planes cannot contain ions of exclusively

one sign also applies. Consequently the slip mode for ionic crystals of the CsCl lattice is not {100} ⟨001⟩ but rather {110} ⟨001⟩. It is therefore expected that highly ionic B_2 type of alloys for which necessarily $\gamma_A \geq \gamma_{A_1}$, exhibit the {110} ⟨001⟩ mode of slip. Intimate cross-slip of the a[001] dislocation on (110) and ($\bar{1}$10)planes, however, can lead to slip bands on various planes of the [001] zone. It is also possible that less ionic B_2 alloys might also slip by the {100} ⟨001⟩ mode and thus permit the a[001] dislocation to cross-slip between (100), (010), (110) and ($\bar{1}$10) planes.

Predicted modes of slip based on the above analyses are given in Table I for a number of completely ordered B_2 alloys ($n^2 = 1$) for which comparative experimental data are available. The bond ordering energy, ϵ, of Table I was estimated in the following way.

For those alloys that disordered below their melting temperature, ϵ, was determined from their Curie temperature, T_c, as suggested by the Bragg-Williams[10] theory namely

$$\epsilon = -\frac{kT_c}{4} \tag{8}$$

where T_c is the critical disordering temperature and k Boltzmann's constant. An upper bound to the ordering energy for alloys that melt before they disorder is given by

$$\epsilon \lesssim -\frac{kT_m}{4} \tag{9}$$

where T_m is the melting temperature.

In general the theoretically predicted modes of slip are confirmed experimentally. The minor exceptions that have been noted might be due to the theoretical approximations introduced by using isotropic elasticity and nearest neighbor bond energies. They might also arise from the asymmetric behavior exhibited by some ordered B_2 alloys.

TABLE I Predicted Modes of Slip

B_2 alloy	Lattice Parameter $a \times 10^8$ cm	Shear Modulus $G \times 10^{-10}$ dynes/cm^2	Bond Ordering Energy ϵ ergs	
			$-\frac{kT_c}{4}$	$< -\frac{kT_m}{4}$
B-Cu-Zn	2.954	13.70	-2.546×10^{-14}	--
β'-AgMg	3.310	18.40	--	$< -3.77 \times 10^{14}$
β'-NiAl	2.881	44.5	--	$< -6.59 \times 10^{-14}$

Antiphase-Boundary Energy, γ, ergs/cm^2				
γ_A			$\gamma_{A_1}^*$	$\gamma_{A_2}^*$
{110}	{112}	{123}		
0.825×10^2	0.953×10^2	0.934×10^2	0.056×10^2	5.57×10^2
0.973×10^2	1.14×10^2	1.10×10^2	0.084×10^2	8.40×10^2
22.46×10^2	25.92×10^2	25.40×10^2	0.178×10^2	17.67×10^2

*γ_{A_1} and γ_{A_2} were calculated for screw dislocations, i.e. taking $\nu=0$

Predicted		Experimentally Determined	
Slip vector	Slip plane	Slip vector	Slip Plane
⟨111⟩	{110}	⟨111⟩	{110}[1,2,5]
⟨111⟩	{110}, {112}	⟨111⟩	{112}[9]
		⟨001⟩*	{110}*
⟨001⟩	{110}	⟨001⟩	{110}[7]

*Present results

Another debatable issue in the deformation of bcc metals and many of their solid-solution alloys is the temperature dependence of yield and flow stresses. Most observations have revealed that bcc metals and many of their solid-solution alloys, in general, have a strong temperature dependence of yield and flow stress. This is frequently attributed to the large Peierls stress inherent in the bcc lattice at low temperatures. Mukherjee and Dorn[11] have investigated the temperature and strain rate dependence of the flow stress of AgMg single crystals in orientation near the [001] direction. The authors found that the calculated values of the associated activation energies and activation volumes were consistent with the theoretical dictates of the Dorn-Rajnak[12] formulation of the Peierls mechanism where the deformation is controlled by the rate of nucleation of pairs of dislocation kinks over the Peierls energy barriers. However, non-crystallographic {hk0} ⟨001⟩ slip in β'-phase AuZn[13] was explained in terms of thermally activated cross-slip of screw dislocations from sessile to glissile configurations.

The study of work hardening of long range ordered alloys and intermetallic compounds that crystallize in the B_2 lattice (CsCl type structure) is still not frequent. It is known (Flinn,[8] Marcinkowski and Miller,[14] Vidoz[15] et al.) that an alloy which possesses long-range order work-hardens more rapidly than the same alloy when it is disordered. Vidoz and Brown[16] have extended the jog theory, developed by Hirsch[17] and Hirsch and Warrington,[18] to the work-hardening situation in superlattice alloys. These authors pointed out that if a superdislocation which consists of two partial dislocations in the superlattice joined by a strip of antiphase-boundary (APB), is jogged, it is probable that the jogs on the superpartials will not be aligned. When this happens a tube of antiphase-

boundary (APB) will be created behind moving superdislocations which will lead to an additional drag on the dislocation, and hence to an increased work hardening rate in relation to disordered material. Investigation of strain hardening by Wood and Westbrook[19] and of stored energy and resistivity by Robinson and Bever[20] in polycrystalline intermetallic compound AgMg indicated that the rate of strain hardening of ordered stoichiometric alloys is greater than that of non-stoichiometric alloys. Furthermore, their results showed that for a given strain, the strain induced destruction of order is greater in non-stoichiometric than in stoichiometric alloys. These authors concluded that the halves of superdislocations in the non-stoichiometric alloys are widely separated and move independently creating ribbons of antiphase-boundary (APB), while in the stoichiometric alloy the superdislocation halves move as a unit. As discussed by Flinn,[8] Bragg[21] and Cupschalk and Brown,[22] antiphase domains in the CsCl structure are unstable and a domain network would not be present in alloys of this structure annealed below the critical ordering temperature. Consequently an increase in strain hardening rate resulting from the cutting of domain walls by mobile superdislocations would not be expected in intermetallic compound AgMg (CsCl type structure).

The present investigation was undertaken with the major objective of establishing experimentally the effect of orientation and temperature on slip geometry, yielding and strain hardening behaviors of AgMg single crystals. To investigate whether there is an asymmetry in yielding and strain hardening, orientations near the [001] direction and near the [$\bar{1}$11]-[011] boundary were selected for study. From Schmid-factor considerations, these orientations are the most conducive to {112} slip. A consideration of the crystallography of slip on this plane shows that for

these orientations the senses of slip in the ⟨111⟩ direction are opposite in tension and compression. A second objective was to elucidate the mechanism of strain hardening of AgMg single crystals.

II. EXPERIMENTAL PROCEDURE

The AgMg alloy was produced by vacuum melting high purity Ag(99.995 wt. pct) and high purity Mg(99.997 wt. pct.) together in a graphite crucible and chill casting in a water cooled copper mold to prevent segregation. Single crystals of AgMg were grown from the cast ingots by a modified Bridgeman technique. Spherical single crystals were first grown in a graphite mold under argon atmosphere. The spheres were then rotated to the desired orientation by means of a two circle goniometer fixture as determined by back reflection Laue x-ray analysis. The oriented spheres were partly melted and cylindrical seed crystals were then grown. From these seeds cylindrical crystals were grown. Crystals were machined into tensile specimens of the following dimensions: total length 3.0 inch, gauge length 1.0 inch, square cross-section of 0.175 inch × 0.175 inch. The shoulder radius was 0.125 inch (Fig. 2a). Compression specimens of dimensions: 0.220 × 0.220 × 0.692 inch (Fig. 2b) were also machined from such crystals. After machining the specimens were electropolished in a solution of 15 grams KCN in 700 ml. of water using 10 volts at about 25°C. The electropolishing was continued until about a 150 micron layer of material was dissolved away in order to ensure that all deformation put into the specimens during machining was removed. These specimen were then annealed in vacuum for 3 hours at 600°C. The annealed specimens were electropolished again prior to testing. X-ray Laue patterns of the surfaces of the annealed specimens indicated that all observable surface mechanical damage was removed.

The composition of the single crystal specimens was chemically analysed for Ag and Mg content. Samples for analysis were taken from

two extreme ends of the gauge length in order to ascertain the variation in composition along the gauge length. Table II shows the results of the chemical analysis. The stoichiometric AgMg compound contains 81.6 wt. pct. Ag. It was obvious that during melting, in order to grow single crystals specimens of AgMg, there had been some loss of Mg with a consequent increase in Ag content. But the average Ag content was still within 0.43 wt. pct. of the stoichiometric composition and the maximum variation of the Ag content from one specimen to another was less than 0.25 wt. pct.

Tensile tests were carried out on a standard Instron machine (shear strain rate $\gamma = 1.67 \times 10^{-5} \text{sec}^{-1}$) at different temperatures. Compression tests at 237.5°K were carried out in a compression jig fitted into the standard Instron testing machine. The yield stress was determined to within 30 psi, and tensile strains were calculated to within ± 0.0001, from the Instron crosshead speed. Test temperatures were obtained by complete immersion of the specimens into different constant-temperature baths. Tension tests conducted below 77°K were carried out in a special cryostat. Back-reflection Laue x-ray patterns were taken of all deformed crystals to determine the rotation of the tensile and compressive axes. Several specimens were x-rayed after various amounts of deformation to follow the rotation of the crystal during straining. The slip lines were observed using the Normarski interference contrast technique. Operative slip systems were determined by the two surface trace analysis method. Orientations investigated are shown in (Fig. 3a).

TABLE II

Analysis of specimen tested at	%Mg	Difference between top and bottom %Mg	%Ag	Difference between top and bottom %Ag
77°K	Top 17.75 Bottom 17.99	0.24	Top 82.02 Bottom 81.91	0.11
153°K	Top 17.85 Bottom 17.92	0.07	Top 82.00 Bottom 82.14	0.14
237.5°K	Top 17.76 Bottom 17.79	0.03	Top 81.99 Bottom 82.12	0.13

III. EXPERIMENTAL RESULTS

Various orientations within the standard stereographic triangle were investigated as shown in Fig. 3a. The orientation of the specimens was specified by the angles λ and χ' shown in Fig. 1. The angle χ'_0, represents the angular rotation of the plane of maximum resolved shear stress from the $(\bar{1}10)$ plane. The angle ψ_0, represents the angular rotation of the observed slip plane from the reference $(\bar{1}10)$ plane and the angle λ_0 is the Schmid angle for slip in the [001] direction for orientation (⊗). The angle χ'_1, is the angle between the maximum resolved shear stress plane and a reference $(\bar{1}01)$ plane. The angle ψ_1, is the angle between the observed slip plane and the reference $(\bar{1}01)$ plane and λ_1 is the Schmid angle for slip in the [111] direction for orientation (⊗). Similar angular relationships hold for $[\bar{1}11]$ slip direction.

General observation of the mechanical data for specimens tested in tension indicates that the temperature dependence of the flow stress varies with respect to tensile orientation. The flow stress was found to vary vastly with temperature for orientations near the [001] direction, while for orientations near the $[\bar{1}11]$-[011] boundary, the flow stress was relatively independent of temperature over the range from 50°K to 300°K. The relationship between the flow stress and temperature for different orientations is shown in Fig. 4. At high temperatures (≈ 237.5°K), for orientations near the [001] direction (e.g. orientations L, C, J, Fig. 3a), slip lines were observed to be coarse, long, not evenly spread through the gauge section, and crystallographic (Figs. 8a, 8c, and 9b). Cross-slip was evident (as shown in Figs. 8e, 9a, and 9b). For orientations near the $[\bar{1}11]$-[011] boundary (e.g. orientations A, B, D, and E) at

higher temperatures ($\approx$ 237.5°K), the slip traces on the face were generally short and wavy, while those on the side were long and straight (Figs. 10a, and 11a). Slip traces were found to be non-crystallographic and to fall on high-indexed planes in the zone of the slip direction [001]. At low temperatures ($\approx$ 77°K), slip traces on both faces were rather straight and fell on low-indexed planes (Figs. 10c, and 11b). Slip traces were detected at strains as low as 0.5% with the aid of the Normarski interference contrast technique (resolution limit 3×10^{-4} cm) for orientations near the [001] direction. At this low strain only one operative slip plane was detected near the center of the specimen. At higher strains other slip traces were detectable throughout the specimen. At 237.5°K, and for orientations near the [001] direction (e.g. orientation L), the strain for the observed onset of secondary slip traces was about 5% or more. For specimens in orientations near the [$\bar{1}$11]-[011] boundary (e.g. orientations A, B, and E) slip traces were detected at strains as low as 3%.

A. Effect of Orientation and Temperature on Flow Stress

1. Effect of Temperature

A strong temperature dependence of the tensile flow stress was observed for crystals in orientations near the [001] direction (e.g. orientation J), while for crystals oriented near the [$\bar{1}$11]-[011] boundary (e.g. orientations E and D) the tensile flow stress was relatively independent of temperature over the range from 50°K to 300°K (as shown in Fig. 4). Below 50°K, crystals in orientation (E) exhibited a striking change in the tensile flow stress. The tensile flow stress increased rather abruptly to a value about twice as much as that at 77°K (Fig. 4).

Similar behavior was exhibited by crystals in orientation (D). As shown in Fig. 4, the athermal stress level $\tau_{237.5^\circ K}$ for crystals in orientations near the [$\bar{1}$11]-[011] boundary is higher than that for crystals in orientations near the [001] direction. This stress level for all annealed specimens varies between about 7.719×10^3 psi for crystals in orientations near the [$\bar{1}$11]-[011] boundary (e.g. orientations E, and D) to about 5.192×10^3 psi for crystals in orientations near the [001] direction (e.g. orientation J).

2. Effect of Orientation

In studying the effect of orientation on the flow stress, crystals in various orientations within the standard stereographic triangle (Fig. 3a) were tested in tension and compression at 237.5°K and shear strain rate 1.76×10^{-5} sec^{-1}. For orientations near the [$\bar{1}$11]-[011] boundary, the orientation dependence of the tensile flow stress resolved on the macroscopic slip plane in the zone of the [001] slip direction is summarized in Table III. Although some scatter in the results is evident, the resolved shear stress τ_T, is approximately independent of orientation. For crystals oriented near the [001] direction, the orientation dependence of the tensile flow stress resolved on the macroscopic slip plane in the zone of the [$\bar{1}$11] slip direction is given in Table IV. The resolved shear stress, τ_T, is also approximately independent of orientation. In general, the resolved shear stress, τ_T decreases from about 7.719×10^3 psi to about 5.192×10^3 psi on moving from near the [$\bar{1}$11]-[011] boundary, where [001] slip is observed, to near the [001] direction, where [$\bar{1}$11] slip is observed. The orientation dependence of the resolved shear stress, τ_c, for crystals in orientations near the [$\bar{1}$11]-[011] boundary deformed in compression at 237.5°K is shown in

TABLE III Effect of Orientation on the Resolved Shear Stress, τ_T, for Crystals in Orientation Near the $[\bar{1}11]$-[011] Boundary. ($T = 237.5°K$, $\gamma = 1.67 \times 10^{-5}$ sec^{-1})

Orientation Ref. Fig. 3a	λ_0 = the Schmid Angle for slip in the [001] direction	χ_0' = the angle between the plane of max. shear stress and (110)	Tensile yield stress resolved on the macroscopic slip plane in the zone of the [001] direction $\times 10^3$ psi ±30 psi
A	43°	+23°	7.968
B	48°	+ 7°	7.972
1B	35°	+17°	7.705
D	42°	+ 9°	7.574
E	42°	+32°	7.870
G	43.5°	+42°	7.984
H	46.5°	+27°	7.600
I	48.5°	+19°	7.702
K	33°	+45°	7.400
R	38°	+ 6°	7.418

TABLE IV Effect of Orientation on the Resolved Shear Stress τ_T, for Crystals in Orientations Near the [001] Direction ($T = 237.5°K$, $\gamma = 1.6 \times 10^5 sec^{-1}$)

Orientation Ref. Fig. 3a	λ_2' = the Schmid angle for slip in the [111] direction	χ_2' = the angle between the plane of max. shear stress and (101)	Tensile yield stress resolved on the macroscopic slip plane in the zone of the [$\bar{1}$11] slip direction ×10 psi ± 30 psi
C	29°	-26°	4.608
F	38°	± 1°	5.585
J	37°	-24°	5.116
M	35°	- 5°	5.569
L	40°	-11°	5.080

TABLE V. Effect of Orientation on the Resolved Shear Stress, τ_c, for crystals in orientations near the [$\bar{1}$11]-[011] boundary (T = 237.5°K, $\gamma = 1.67 \times 10^{-5} sec^{-1}$)

Orientation Ref. Fig. 3a	λ_1' the Schmid angle for slip in the [111] direction	χ_1' = the angle between the plane of max. shear stress and ($\bar{1}$01)	Compressive yield stress resolved on the macroscopic slip plane in the zone of the [111] slip direction ×10 ± 30 psi
G	38°	+26°	5.050
K	37.5°	+ 9°	5.085
R	60°	+15°	5.095

Table V. It follows from Tables IV and V that the resolved shear stress values in tension and compression are related by

$$\tau_{(112)[111]}^{(T)} = 1.023\ \tau_{(211)[111]}^{(C)}$$

It also follows from Tables III and V that crystals in orientations near the $[\bar{1}11]$-[011] boundary, deformed in tension and compression at 237.5°K, exhibit asymmetry in the resolved shear stress for slip on {112} planes. Crystals oriented near the [001] direction also exhibit asymmetry in the resolved shear stress for slip on {112} planes under tension and compression at 237.5°K.

B. Effect of Orientation and Temperature of the Slip System

1. Effect of Orientation

The dependence of ψ (Fig. 1) on orientation was studied for crystals in various orientations within the standard stereographic triangle (Fig. 3a) tested in tension and compression at 237.5°K and shear strain rate 1.67×10^{-5} sec^{-1}. The 237.5°K dependence of ψ_0 on orientation for crystals in orientations near the $[\bar{1}11]$-[011] boundary tested in tension at a shear strain rate 1.67×10^{-5} sec^{-1} is plotted in the form of a $\psi_0(\chi_0')$ curve in Fig. 7a. The figure shows that slip occurs generally on non-crystallographic planes $(\sim\bar{1}20)$ in the zone of the [001] direction except in the approximate range $+40° < \chi_0' \leq +45°$.

One special feature worth mentioning is the fact that $(\bar{2}11)$ slip was never observed when crystals of orientation E, where the (211) plane is most highly stressed, were deformed in tension at 237.5°K. $(\bar{2}11)$ slip was observed when crystals in this orientation were tested in compression at 237.5°K. This suggests that the $(\bar{2}11)$ plane has a high critical stress for slip in tension and a low critical stress for slip

in compression for crystals in orientation E deformed at 237.5°K.

The effect of orientation on ψ_2 for crystals in orientations near the [001] direction tested in tension at 237.5°K and shear strain rate 1.67×10^{-5} sec^{-1} is shown in Fig. 7b, in which the slip plane is plotted as a function of orientation in the form of a $\psi_2(X_2')$ curve. Slip was found to occur on $(1\bar{1}2)[\bar{1}11]$ system. Figures 8a, 8e and 9b show examples of $(1\bar{1}2)[\bar{1}11]$ slip system at 237.5°K.

The 237.5°K dependence of ψ_1 on orientation for crystals in orientations near the $[\bar{1}11]$-[011] boundary (e.g. orientations A, B, G, K, Fig. 3a) tested in compression at shear strain rate 1.67×10^{-5} sec^{-1} is plotted in Fig. 7c. Slip was observed to be on the $(\bar{2}11)[111]$ system. Examples of the $(\bar{2}11)[111]$ slip system are shown in Figs. 12b and 12c. The 237.5°K dependence of slip systems on orientation under tension and compression is summarized in Figs. 3b and 3c respectively.

2. <u>Effect of Temperature</u>

The effect of temperature on the slip system for crystals having different orientations within the standard stereographic triangle has also been studied. The effect of temperature on the slip system for crystals in orientation near the [001] direction (orientation J) tested in tension at a shear strain rate of 1.67×10^{-5} sec^{-1} is shown in Fig. 7d. Slip was found to take place on the $(1\bar{1}2)[\bar{1}11]$ system in the range from 20°K to 300°K. Figures 9a, 9b and 9c show examples of the $(1\bar{1}2)[\bar{1}11]$ system at different temperatures. The effect of temperature on the slip plane for the (hk0)[001] system is plotted in Fig. 7e for crystals of two orientations (E and D, Fig. 3a) deformed in tension in the range from 50°K to 300°K. Since generally $\psi_0' \neq X_0'$, the slip plane is not the

plane of highest resolved shear stress in the [001] zone. Below 50°K, crystals in orientation E exhibited a striking change in the observed slip system. [111] slip on the ($\bar{2}$11) plane was observed (as shown in Figs. 11d and 11e).

C. Effect of Orientation and Temperature On the Strain Hardening of AgMg Single Crystals

1. Effect of Orientation

The strain hardening behavior of crystals having various orientations within the standard triangle tested in tension and compression at 237.5°K and shear strain rate 1.67×10^{-5} sec^{-1} is shown in Fig. 6. These results show a significant difference in the strain-hardening behavior between crystals with tensile-axis orientation near the [001] direction and those oriented near the [$\bar{1}$11]-[011] boundary. As shown in Fig. 6 the strain hardening behavior of AgMg single crystals at 237.5°K is very orientation dependent. For crystals with tensile-axis orientations near the [001] direction (e.g. orientations J, L, and M) deformed in tension at 237.5°K and shear strain rate 1.67×10^{-5} sec^{-1}, the stress-strain curves are characterized by a short region of easy glide (Stage I), followed by a linear region of relatively low rate of strain hardening (Stage II). The strain-hardening rate increases gradually during the transition from Stage I to Stage II and then becomes fairly constant. Slip-line observations were made after various amounts of tensile deformation at 237.5°K on crystals in orientation L, Fig. 3a. In Stage I, slip traces were observed to be very coarse, long, and not evenly spread through the gauge section as shown in Fig. 8a. Polishing followed by increments of tensile strain in Stage II revealed slip traces which appeared to be broken up into relatively fine and more evenly spread traces through the gauge

section Fig. 8c. Stage I was observed to end well before the onset of any double glide. Furthermore, for crystals in orientations J and C tested in tension at 237.5°K, $(1\bar{1}2)$-$(2\bar{1}3)$ cross-slip was evident as shown in Figs. 8e and 9b. In contrast, upon reversing the sign of the applied stress i.e. from tension to compression, crystals oriented near the [001] direction (e.g. orientation P, Fig. 3a) yielded parabolic stress-strain curves with high rates of strain hardening as shown in Fig. 6.

Crystals with axis orientations near the $[\bar{1}11]$-[011] boundary (e.g. orientations D, E and I) deformed in tension at 237.5°K, exhibited parabolic stress-strain curves with high rates of strain hardening (Fig. 6). In contrast, upon the change of the sign of the applied stress from tension to compression, crystals in these orientations yielded classical single crystal stress-strain curves with relatively low Stage II hardening (Fig. 6).

Crystals in orientations F, and 1B yielded a transition strain hardening behavior during deformation as shown in Fig. 6. Primary slip was observed to occur on the $(1\bar{1}2)[\bar{1}11]$ system (Fig. 8d). The high strain-hardening rate exhibited by crystals in these orientations was associated with [001] slip. It follows from the present results that AgMg single crystals exhibit pronounced asymmetry in the strain hardening behavior under tension and compression.

2. Effect of Temperature

Stress-strain curves of crystals in orientation J deformed in tension in range from 20°K to 237.5°K are shown in Fig. 5. The most significant effect of temperature is that the flow stress increases rapidly with decreasing temperature below 237.5°K. The extent of Stage I (easy glide region) is a maximum at 77°K and decreases with increasing tempera-

ture above 77°K. At 21°K, the stress-strain curve exhibited by crystals in orientation J is irregularly serrated. The observed sharp relaxation in the load at 0.4% tensile strain was accompanied by the formation of deformation band.

Crystals in orientations near the [$\bar{1}$11]-[011] boundary deformed in tension at temperatures between 50°K and 300°K, exhibited parabolic stress-strain curves with high rates of strain hardening as shown in Fig. 5. Below 50°K, crystals in orientation E yielded irregularly serrated stress-strain curves and showed small percentage elongations. The observed sharp relaxations in the load were also accompanied by the formation of deformation bands. These deformation bands appeared to form by a lattice rotation. This conclusion was supported by the detected small splitting of the diffracted spots of back-reflection Laue patterns. This also indicated that the transition between the deformation band and the main lattice was not in the nature of a sharp boundary. On deforming crystals in orientation E at temperature 23°K and 33°K slip traces corresponding to the ($\bar{2}$11)[111] system appeared first, followed by deformation bands at tensile strains as low as 0.15%. Furthermore, the poles of the bands were found to cluster around the [111] direction. The strain-hardening rate of crystals oriented near the [$\bar{1}$11]-[011] boundary appears to be independent of temperature in the range from 50°K to 300°K (Fig. 5).

IV. DISCUSSION OF RESULTS

It has been shown that AgMg single crystals exhibit a highly asymmetric behavior in the resolved shear stress for slip on the {112}⟨111⟩ system and in strain hardening under tension and compression. The orientation dependence of the resolved shear stress on moving from near [$\bar{1}$11]-[011] boundary to near the [001] direction is accompanied by appreciable changes in the strain-hardening characteristics (as shown in Fig. 6). Crystals oriented near the [$\bar{1}$11]-[011] boundary, where the ($\bar{2}$11) plane is most highly stressed, deform in tension by slip in the [001] direction while [$\bar{1}$11] slip on the (1$\bar{1}$2) plane is observed in crystals with axis orientations near the [001] direction. under tension. It has also been shown that crystals in orientations near the [$\bar{1}$11][011] boundary exhibit parabolic stress-strain curves with high rates of strain-hardening, while those oriented near the [011] direction yield classical single crystal stress-strain curves with relatively low Stage II hardening under tension.

Upon reversing the sign of the applied stress from tension to compression, crystals oriented near the [$\bar{1}$11]-[011] boundary exhibit [111] slip on the ($\bar{2}$11) plane, while those in orientations near the [001] direction deform by slip on planes in the zone of the [001] slip direction. The inversion of the yield strength upon the change of the sign of the stress from tension to compression is accompanied by inversion in the strain hardening characteristics. Crystals exhibit classical stress-strain curves with relatively low Stage II hardening under tension, yield parabolic stress-strain curves with high rates of strain hardening under compression, while those exhibit parabolic stress-strain curves with high rates of strain hardening under tension, yield classical stress-strain curves with relatively low Stage II hardening under compression.

(Fig. 6). It is suggested that the equivalence of $(\bar{2}11)[111]$ with $(\bar{1}\bar{1}2)$ $[\bar{1}\bar{1}\bar{1}]$ difficult slip and the equivalence of $(\bar{1}\bar{1}2)[111]$ with $(\bar{2}11)[\bar{1}\bar{1}\bar{1}]$ easy slip lead to the inversion.

To produce slip along the $\langle 111 \rangle$ direction, the superdislocation a[111] must first dissociate into two halves, a/2[111] and a/2[111], linked by a ribbon of antiphase-boundary (APB) in the superlattice, (Fig. 13a), according to

$$a[111] \rightarrow a/2[111] + a/2[111]$$

with a change in the elastic energy per unit length of about $-3/4 \frac{Ga^2}{(1-\nu)}$ where G is the shear modulus of elasticity and ν is Poisson's ratio for edge dislocations and zero for screw dislocations. Each split partial a/2[111] of the superdislocation a[111] in edge orientation can only dissociate asymmetrically on {112} planes Fig. 13b, (Frank and Nicholas)[23] according to the reaction

$$a/2[111] \rightarrow a/3[111] + a/6[111] \qquad (10)$$

The dissociation occurs in such a way that, if the shear stress acts in the sense of twinning, the a/6[111] twinning partial will glide first. Conversely, if the sense of the applied stress is unfavorable for twinning, the complementary partial a/3[111] will glide first. It is expected that the stresses required to move the dislocation in these two cases will be different, since a large energy change is involved in moving the complementary partial a/3[111] first.

It has also been proposed by Hirsch[17] and independently by Sleeswyk[24] that a/2[111] screw dislocations can dissociate into three a/6[111] partials on the {112} planes that intersect along the axis of the original screw dislocation (Fig. 13c) according to the reaction

$$a/2[111] \rightarrow a/6[111] + a/6[111] + a/6[111] \qquad (11)$$

In Fig. (13e) the Burgers vector is assumed to come out of the normal to the plane of the figure. An analysis of the geometry of the partials under the applied stress also predicts that there should be an asymmetry of the stress to move screw dislocations on these planes. The inversion of the yield strength and strain hardening upon the change of the sign of the applied stress from tension to compression, then suggests that when the atoms move in the twinning direction, slip is easy, e.g.[111] slip on the $(\bar{1}\bar{1}2)$ plane under tension, and when the atoms move in the antitwinning direction slip becomes difficult e.g. [111] slip on the $(\bar{2}11)$ plane under tension.

Considering crystals in orientation near the [001] direction (e.g. orientation J) deformed in tension, the direction of the shear stress is such that it would make the twinning partial $a/6[11\bar{1}]$ to glide first and $[\bar{1}11]$ slip on the $(1\bar{1}2)$ plane is then expected to be easy, as evidenced by the results of crystals in this orientation. Similarly, for crystals in orientations near the $[\bar{1}11]$-[011] boundary (e.g. orientation E, and G) under compression, $[\bar{1}\bar{1}\bar{1}]$ slip on the $(\bar{2}11)$ plane is easy as evidenced by the compression results of crystals in these orientation. The present results show that crystals in orientation, J, under tension and those in orientation E, and G under compression, exhibit classical stress-strain curves with relatively low Stage II hardening. It will be shown that the relatively low rate of strain-hardening arises from the elastic and short range interactions of primary dislocations with intersection secondary dislocations.

Considering crystals oriented near the $[\bar{1}11]$-[011] boundary (e.g. orientations D and E) under tension, the sense of the shear stress is

such that it would make the complementary partial a/3[111] to glide first and [111] slip on the $(\bar{2}11)$ plane is then expected to be difficult. Crystals in these orientation exhibit slip on non-crystallographic planes in the zone of the [001] slip direction. The flow stress of crystals in orientations E and D is relatively independent of temperature in the range from 50° to 300°K (as shown in Fig. 4). Furthermore, crystals in these orientations exhibit parabolic stress-strain curves with high rates of strain-hardening (Fig. 5). The high strain-hardening rates appear to be independent of orientation and temperature for crystals oriented near the $[\bar{1}11]$-[011] boundary (Figs. 5 and 6). The difficulty is now to explain the occurance of slip in the [001] direction and the associated high rates of strain hardening.

As mentioned in the introduction, for extremely high values of, γ_A the separation of the two halves, a/2[111] and a/2[111], of the superdislocation will be negligible. Under this condition, the superdislocation can dissociate without change in energy according to

$$a[111] \rightarrow a[110] + a[001]^{*}$$

and (12)

$$a[110] \rightarrow a[100] \pm a[010]$$

Since the Burgers vector of the dissociated parts of the superdislocation are mutually orthogonal, each split dislocation will move independently of the others. In this case slip along [001] direction is expected and the deformation characteristics approach those obtained in CsCl type

*Broon and Humble[25] have observed a⟨110⟩ + a⟨001⟩ dislocation pair lying along ⟨111⟩ direction in a thin foil of beta-brass (CsCl type structure) examined in the electron microscope. The authors concluded that a⟨110⟩ + a⟨001⟩ dislocation pair probably results from the splitting of a⟨111⟩ dislocation, although elastic anisotropy theory predicts that the observed reaction is energetically neutral.

ionic crystals which have extremely high values of antiphase-boundary (APB) energy, γ_A. As shown in Table I, the value of the antiphase-boundary (APB) energies γ_A for AgMg intermetallic compound lies in the range $\gamma_{A_1} \leq \gamma_A \leq \gamma_{A_2}$. In this range of antiphase-boundary (APB) energies, the motion of the two dissociated halves a/2[111] and a/2[111], of the superdislocation are coupled through the intervening antiphase-boundary (APB). Since the two halves of the superdislocation are seperated they cannot recombine and dissociate according to Eq. 12 without the expenditure of recombination energy. Before a sehar stress level* is reached to move the screw dislocation in the antitwinning direction and to give an adequate multiplication rate for crystals in orientation E, where the $(\bar{2}11)$ plane is most highly stressed, in tension, the two dissociated halves a/2[111] and a/2[111], of the superdislocation will recombine over a length, ℓ, as shown in Fig. 13d. Under this condition the a[111] screw dislocation can dissociate without a change in energy into a[110] and a[001] dislocations in accord with Eq. 12. Since for crystals in this orientation, the resolved shear stresses on planes in the [001] zone are high, the [001] dislocation will bow out on $\{\bar{1}10\}$ planes under the action of the shear stress as soon as the recombination of the dissociated halves a/2[111] and a/2[111], of the superdislocation takes place over a length larger than a critical length, ℓ (Fig. 13d). The recombination of the dissociated halves and the subsequent dissociation of the recombined segment of a[111] screw dislocation into a[001] and a[110] dislocations, is the source of the [001] type slip observed in crystals oriented near the $[\bar{1}11]$-[011] boundary under tension. The critical length, ℓ, of the recombined segment

*The shear stress required to move the dislocation in the antitwinning direction is about 8.94×10^3 psi at 237.5°K as evidenced by the results of the compression tests of crystals near the [001] direction (orientation 11, Fig. 3a).

can be estimated from the equation

$$\tau = \frac{2Gb}{\ell} \tag{13}$$

where τ is the shear stress in the direction of the Burgers vector, G the shear modulus of elasticity and b the Burgers vector. By using $\tau = 5.32\times10^{8}$ dynes/cm^2, $G = 18.4\times10^{10}$ dynes/cm^2 ℓ is about 700b. Consequently the stress to recombine the two dissociated halves, a/2[111] and a /2[111], of the superdislocation is athermal, since the energy required to recombine the two dissociated havles over a length larger than the critical length, ℓ 700b, cannot be supplied by thermal fluctuations. Since only few [001] dislocation loops can be nucleated on the $\{\bar{1}10\}$ planes as a result of this mechanism, continued multiplication of the dislocations requires that they cross-slip from and onto $\{\bar{1}10\}$ and {010} planes in the zone of the [001] slip direction. Non-crystallographic slip in the zone of the [001] direction at high temperature ($\approx 237.5^\circ$K) suggests that the screw dislocations can cross-slip without difficulty from and onto $\{\bar{1}10\}$ and {010} planes. At low temperature ($\approx 77^\circ$K) slip is only observed on the (110) plane for crystals in orientations E and D (as shown in Figs. 10c and 11b). This suggests that high friction stress favors $\{\bar{1}10\}$ slip at low temperatures. It then seesm that the multiplication of the [001] dislocations depends on a double cross-slip process when thre stress is sufficiently high to cause cross-slip, and is rather inhibited at low temperatures as evidenced by the rather straight slip lines exhibited by crystals in orientations E and D at low temperatures. During the early stages of deformation the increase in the dislocation density required to maintain the strain rate does not arise from the operation of Frank-Read sources but rather from the operation of new

dislocation sources at higher stress levels (Fig. 13d), and hence high strain hardening rates will be expected, as shown by the results of crystals oriented near the $[\bar{1}11]$-[011] boundary under tension.

For crystals in orientation 11, Fig. 3a deformed in compression at high temperature ($\approx 237.5°K$), the shear on the primary plane is opposite in sense to the twinning shear. Furthermore, the resolved shear stress on planes in the zone of [001] direction for crystals in this orientation approaches zero, and hence slip on planes in the [001] zone will not be expected for this orientation. When the shear stress on the primary plane $(1\bar{1}2)$ reaches a value of 8.9×10^3 psi at 237.5°K, the screw dislocations will tend to move in the antitwinning direction on the {112} planes as evidenced by the results of the compression test of crystals in this orientation. Cross-slip from one {112} to another {112} plane is always difficult, because the leading partial necessarily has the wrong Burgers vector for motion on the cross-slip plane. For crystals in orientation 11 deformed in compression, the shear stress is in the antitwinning direction; the leading partial can dissociate spontaneously, but a constriction has to be made before the cross-slip can be completed. Therefore, these screw dislocations will not easily cross slip and hence the strain hardening rate due to pile-up of dislocations on {112} planes in the antitwinning direction will be expected to be very high as was observed during the early stages of deformation in compression of crystals in orientation 11. As mentioned before, over the temperature range 25°-40°K, crystals in orientations E and D, Fig. 3a deformed in tension exhibited striking changes in the yield stress and the observed slip system. The yield stress was increased rather abruptly to a value twice as much as that at 77°K and the observed slip plane was changed

from $(\bar{1}10)$ to $(\bar{2}11)$. The crystals also exhibited sharp relaxation in the load accompanied by the formation of deformation bands.

The mechanism of formation of these deformation bands in β'-phase AgMg at low temperatures is yet rather uncertain. On deformation, slip on $(\bar{2}11)$ [111] occurred first, followed by deformation bands at tensile strains as low as 0.15% (Fig. 5). If the formation of the deformation bands is a consequence of pile-up of dislocations against a barrier on the slip plane, this barrier must be formed by the deformation. Furthermore, the poles of these bands were found to cluster around the [111] slip direction. This suggests that Mott's[26] edge dislocation wall model may account for their formation. It then seems reasonable to postulate that, in consequence of the rapid piling-up of the dislocations in β'-phase AgMg at low temperatures, plastic deformation is possible only by the formation of deformation bands. However, the rotation of the lattice which generates the deformation bands is crystallographically limited. After exhaustion of the possibility of lattice rotation, brittle fracture will presumably occur, as was observed in crystals in orientations E and D deformed in tension at low temperatures.

It has been shown that the high strain-hardening rate exhibited by crystals in orientation 11 (Fig. 3a), deformed in compression at high temperature ($\approx$237.5 K) is due to the pile-up of screw dislocations on the $(1\bar{1}2)$ plane in the antitwinning direction. However, if the stress rises sufficiently to cause cross slip onto another {112}planes, the screw dislocation on the cross-slip plane will be expected to travel long distance since slip on the cross slip system will be in the twinning direction and the applied stress will relax, possibly giving rise to serrations on the stress-strain curves. This was also observed during

compression of crystals in orientation 11. The above discussion is speculative and only a possible explanation for the observed ⟨001⟩ slip and the associated high rates of strain hardening exhibited by crystals oriented near the [$\bar{1}$11]-[011] boundary.

As shown in Fig. 6 crystal oriented near the [001] direction (e.g. orientation L, M and J) deformed in tension at 237.5°K, exhibit classical single crystal stress-strain curves having a short region of easy glide followed by a linear region of relatively low rate of strain hardening. Crystals in orientations near the [$\bar{1}$11]-[011] boundary (e.g. orientation G) exhibit similar behavior in compression at 237.5°K. The strain-hardening behavior of AgMg single crystals in orientations L, M and J in tension and of those in orientation G in compression at 237.5°K, is similar to that of many bcc metals, for example, Nb (Mitchell, Foxall, and Hirsch)[27] Ta(Mitchell and Spitzig)[28] and Mo (Guiu and Pratt).[29] Although no direct electron-microscopy observations of dislocations in β'-phase AgMg have been made, investigations[27-29] of work hardening of the bcc metals have indicated that the Stage II hardening mechanism is generally based on a model of primary dislocation groups piled-up against obstacles. However, because of internal stresses, secondary dislocations could be generated around the tips of these piled-up groups, converting the piled-up dislocations into tangles, which in turn would inhibit further slip. It is still doubtful however, whether pile-up groups form, especially in Stage I and subsequently decompose into tangles. The question of the origin and nature of secondary dislocations is interesting and worth speculation.

Hirsch and others (Hirsch,[30] Mitchell,[31] Basinski and Mitchell[32]) have pointed out that secondary dislocations can form by relaxation of the stress at tips of pile-ups of primary dislocations. These dislocations do not have to contribute appreciably to macroscopic strain on the secondary system because their movements are very restricted and because these localized secondary dislocation groups could consist of positive and negative dislocations ofnearly equal density. On the other hand, the applied stress generally has a shear component on the secondary system. This shear component will become larger as the deformation proceeds, and this increase could be a factor in the operation of secondary sources. The observation that the strain for the onset of secondary slip traces of crystals in orientation L is about 5.0% or more (Fig. 6) tends to support this hypothesis. It is then likely that the relatively low rate of strain hardening in Stage II (linear hardening region) is due mainly to elastic and short range interactions of primary dislocations with intersecting secondary dislocations. The very low hardening rate in Stage I (easy glide region) appears to be due to glide of dislocations on a single slip system with very little interference from secondary systems. Cross-slip of screw dislocations seems to be easy as evidenced from the slip traces of crystals in orientation J(Fig. 9b), and this can further aid the ease of movement of dislocations through the crystal.

Vidoz and Brown[16] have proposed a temperature independent work hardening model for ordered alloys which is based on the creation of antiphase-boundary (APB) tubes during glide of superdislocation pairs that contain non-aligned jogs formed by the mutual intersection between mobile superdislocations. The process of the formation of antiphase-boundary (APB) tubes on gliding superdislocations is illustrated in Fig. 14. Each half of a glide superdislocation that has intersected a forest dislocation in screw orientation will acquire two jogs. The distance between jogs will depend on the separation, y, of the halves of the forest superdislocations and on the geometric arrangements of the pairs of superdislocations upon intersection. The jogs on the trailing half of the dislocation will be displaced a distance, d, from those on the leading half whenever the forest superdislocation moves in its slip plane during the process of intersection. In this event, subsequent motion of the superdislocations will produce two rectangular tubes of antiphase boundary (APB). The distance ℓ_j between the pairs of tubes will depend on how many jogs forming forest dislocations are intersected.

When the superdislocations are in screw orientation, the jogs can glide along the dislocation conservatively. But since the jogs on each half of the superdislocation have the same sign, they may because of their mutual repulsions move apart. Since the jogs on each half of the superdislocation in screw orientation can glide along the dislocation lines they might be pulled due to the APB energy into alignment during motion of the superdislocation, thereby pinching off the APB tubes. The jogs however will leave a trial of vacancies or interstitials behind them as they are pulled forward with the dislocations.

When the superdislocations is in edge orientation, the jogs cannot glide conservatively along the dislocation. In this case the APB tubes cannot pinch off. However, the jogs can glide forward conservatively with the moving superdislocation. In general a superdislocation having both screw and edge character will exhibit an appropriate average behavior between that for pure screw and that for pure edge dislocation. When the pairs of tubes are a distance ℓ_j apart, the stress required to move the dislocation is

$$\tau_T = \tau_G + \frac{2\gamma d}{b\ell_j} \qquad (14)$$

where τ_G is the stress required to overcome interactions between dislocations, γ is the energy per unit area of the antiphase-boundary (APB) and b is the Burgers vector.

It has been shown that the high strain-hardening rates exhibited by crystals oriented near the [$\bar{1}$11]-[011] boundary deformed in tension at 237.5°K was associated with slip on planes in the zone of the [001] direction. [001] slip implies that the deformation proceeds without the formation of antiphase-boundaries (APB) and hence without disordering the lattice. Consequently, the motion of the [001] dislocations on the glide plane will not produce tubes of antiphase-boundary (APB). Therefore, the high rates of strain-hardening exhibited by crystals in these orientations cannot be expected to be due to the formation of tubes of antiphase-boundaries (APB^S).

It has also been shown that crystals in orientations near the [001] direction (e.g. orientations L, M and J) deformed in tension and those in orientation near the [$\bar{1}$11]-[011] boundary (e.g. orientation G) deformed in compression at 237.5°K, yielded classical single crystal stress-strain

curves having a linear region of relatively low strain-hardening rate. For crystals in these orientations, primary slip was observed on the $(1\bar{1}2)[\bar{1}11]$ system; secondary slip on the $(\bar{1}\bar{1}2)[111]$ system. In this case the superdislocations on the two active slip planes have different Burgers vectors and mutual interactions will produce unit jogs on the dislocations. Thus high rates of strain-hardening would be expected as a result of the formation of jogs on the superdislocations on the $(1\bar{1}2)[\bar{1}11]$ primary slip system resulting from intersections with superdislocations moving on the $(\bar{1}\bar{1}2)[111]$ secondary system. Consequently, the relatively low rates of strain-hardening exhibited by crystal in these orientations do not appear to be due to the formation of antiphase-boundary (APB) tubes on mobile superdislocations as suggested by Vidoz and Brown. Furthermore, the present results show that crystals in orientation F (Fig. 6) exhibit a transition strain hardening behavior during tensile deformation. Crystals in this orientation, where deformation occurred by the simultaneous operation of two slip systems $(\bar{1}\bar{1}2)[\bar{1}11]$ and $(\bar{1}\bar{1}2)[111]$ having different Burgers vectors, initially exhibit low rates of strain hardening. The rapid increase in the strain-hardening rates is associated with slip in the [001] direction. The tensile deformation of these crystals further shows that the high rates of strain-hardening is not due to the formation of tubes of antiphase-boundaries on mobile superdislocations. For crystals in orientation F, tensile deformation by slip on the primary $(1\bar{1}2)[\bar{1}11]$ system produces crystal rotation that increases the resolved shear stress on the $(\bar{2}11)$ plane. The high strain-hardening rate is then due to the athermal recombination of the dissociated halves, a/2[111] and a/2[111], of the superdislocation and the subsequent dissociation of the recombined segment of a[111] screw dislocation into a[110] and a[001] dislocations.

The effect of temperature on the stress-strain curves yielded by crystals in orientation near the [001] direction (e.g. orientation J) is observed to be that, as the temperature increases above 77°K, the extent of the easy glide region (Stage I) decreases while that of the linear hardening region (Stage II) increases, as shown in Fig. 5. This suggests that the operation of secondary sources may be aided by thermal fluctuations. Thus the relatively low hardening rates observed during the deformation of crystals oriented in the [001] direction (e.g. orientations L, M and J) in tension and of those oriented near the [$\bar{1}$11]-[011] boundary in compression appear to be consistent with the strain-hardening model based on the elastic and short range interactions of primary dislocations with intersecting secondary dislocations. However, since at the present time no detailed electron microscope observations are available on the nature of the dislocation structure in deformed AgMg single crystals, a complete model accounting for every detail of the plastic behavior will have to wait unit much more knowledge about the arrangements of the dislocations is gained.

V. SUMMARY

1. The plastic behavior of AgMg single crystals of various orientations in the standard stereographic triangle has been investigated in tension over the range from 20°K to 300°K and in compression at 237.5°K. The critical resolved shear stress for slip on the {112} planes and the strain hardening are found to be asymmetric.

2. Crystals oriented near the [001] direction deform in tension by slip in the $[\bar{1}11]$ direction and on well defined crystallographic planes $(1\bar{1}2)$ in the range from 20°K to 300°K, while those oriented near the $[\bar{1}11]$-[011] boundary deform in tension by slip on a system of the form {hk0} ⟨001⟩. Crystals oriented near the $[\bar{1}11]$-[011] boundary deform in compression by slip on the $(\bar{2}11)$[111] system.

3. Crystals oriented for ⟨111⟩ slip exhibit classical single crystal stress-strain curves with relatively low Stage II hardening, whereas crystals oriented for ⟨001⟩ slip yield parabolic stress-strain curves with high rates of strain hardening.

4. The high rates of strain-hardening exhibited by AgMg single crystal is qualitatively explained in terms of a model based on the athermal recombination of the dissociated halves a/2[111] and a/2[111], of the superdislocation and the sebsequent dissociation of the recombined segment of a[111] screw dislocation into a[110] and a[001] dislocations. The relatively low rates of strain hardening are due mainly to elastic and short-range interactions with the intersecting dislocation.

5. The strain hardening behavior of AgMg single crystals does not appear to be due to Vidoz-Brown mechanism of forming athermal barriers to the motion of superdislocations by the creation of tubes of antiphase boundary as a result of jogs formed by the intersection with mobile forest superdislocation.

ACKNOWLEDGEMENTS

The author is very grateful to Professor John E. Dorn for his guidance and encouragement during his graduate studies and this investigation, to Professor S. Frederick Ravitz for his continuous interests and guidance.

Thanks are also due to Dr. Jack B. Mitchell for manuscript review and helpful discussions during the coarse of this work, Mrs. G. Pelatowski for line drawings and to Miss Jane Ball for typing this report.

This work was done under the auspices of the United States Atomic Energy Commission through the Inorganic Materials Research Division of the Lawrence Radiation Laboratory.

REFERENCES

1. W. A. Rachinger and A. H. Cottrell, Acta Met., 1956, Vol. 4, p. 100.

2. G. I. Taylor, Proc. Roy. Soc. A., 1928, Vol. 118, p.1.

3. H. L. Burghoff, Trans. AIME, 1940, Vol. 137, p. 214.

4. A. B. Greninger, Trans. AIME, 1938, Vol. 128, p. 368.

5. A. Ball and R. E. Smallman, Acta Met., 1966, Vol. 14, p. 1517.

6. A. Ball and R. E. Smallman, Acta Met., 1966, Vol. 14, p. 1349.

7. R. J. Wasilewski, S. R. Butler and J. E. Hanlon, Trans AIME, 1967, Vol. 239, p. 1357.

8. P. A. Flinn, Trans. AIME, 1960, Vol. 218, p. 145.

9. V. B. Kurfman, Acta Met., 1965, Vol. 13, p. 307.

10. W. L. Bragg and E. J. Williams, Proc. Roy Soc. A, 1934, Vol. 145, p. 699.

11. A. K. Mukherjee and J. E. Dorn, Trans. AIME, 1965, Vol. 233, p. 652.

12. J. E. Dorn and S. Rajnak, Trans. AIME, 1964, Vol. 230, p. 1052.

13. E. M. Schulson and E. Teghtsoonian, Phil. Mag., 1969, Vol. 19, p. 155.

14. M. J. Marcinkowski and D. S. Miller, Phil. Mag., 1961, Vol. 6 p. 871.

15. A. E. Vidoz, D. P. Lazarevic and R. W. Cahn, Acta Met., 1963, Vol. 11 p. 17.

16. A. E. Vidoz and L. M. Brown, Phil. Mag., 1962, Vol. 7, p. 1167.

17. P. B. Hirsch, 1960, Fifth Intern. Congr. Crystallography, Cambridge England.

18. P. B. Hirsch and D. Warrington, Phil Mag., 1961, Vol. 6, p. 735.

19. D. L. Wood and J. H. Westbrook, Trans AIME, 1962, Vol 224, p. 1624.

20. P. M. Robinson and M. B. Bever, Acta Met., 1965, Vol. 13, p. 647.

21. W. L. Bragg, Proc. Phys. Soc. London, 1960, Vol. 57, p. 105.

22. S. G. Cupschalk and N. Brown, Acta Met., 1967, Vol. 15, p. 847.

23. F. C. Frank and J. F. Nicholas, Phil. Mag., 1953, Vol. 44, p. 1213.

24. A. W. Sleeswyk, Phil. Mag., 1963, Vol. 8, p. 1467.

25. N. Broom and P. Humble, 1968, Commonwealth Scientific and Industrial Research Organization, Division of Tribophysics, University of Melbourne, Australia.

26. N. F. Mott, Proc. Phys. Soc. B, 1951, Vol. 64, p. 729.

27. T. E. Mitchell, R. A. Foxall and P. B. Hirsch, Phil Mag., 1963, Vol. 9, p. 1895.

28. T. E. Mitchell and W. A. Spitzig, Acta Met., 1965, Vol. 13, p. 1169.

29. G. Guin and P. L Pratt, Phys. Stat. Sol., 1966, Vol. 15, p. 539.

30. P. B. Hirsch, Disc. Faraday Soc., 1964, Vol. 38, p.111.

31. T. E. Mitchell, Phil. Mag., 1964, Vol. 10, p. 315.

32. Z. S. Basinski and T. E. Mitchell, Phil Mag., 1966, Vol. 13, p. 103.

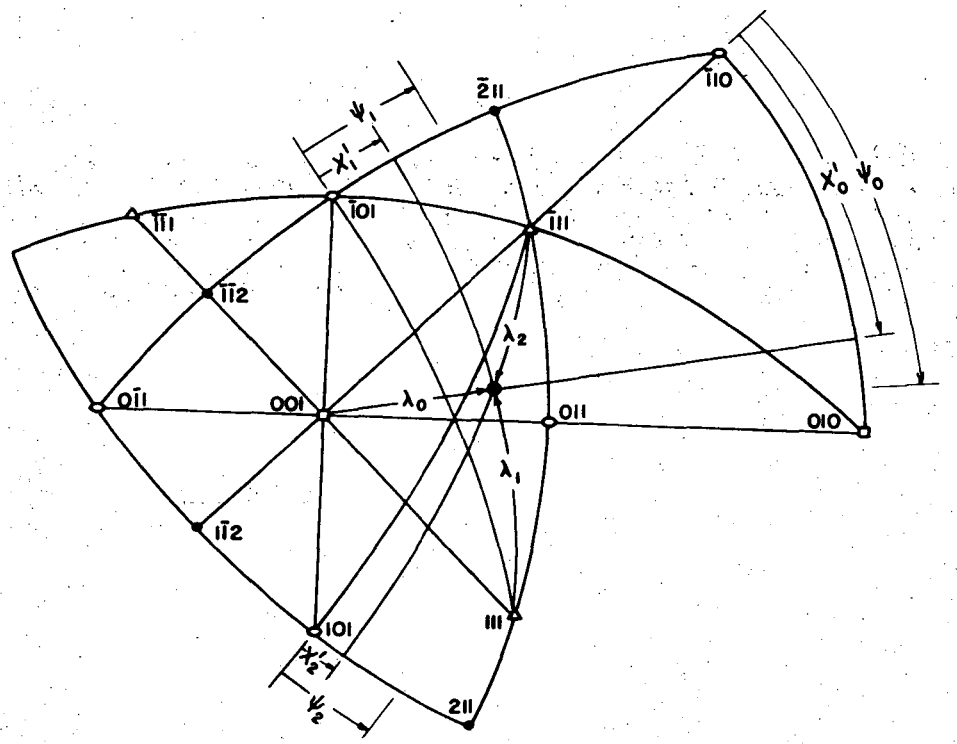

FIG. 1 [001] STEREOGRAPHIC PROJECTION. (● IS THE POLE OF THE SPECIMEN AXIS; ψ_0 AND χ_0' ARE THE ANGLES THAT THE OBSERVED PLANE OF SLIP AND THE PLANE OF MAXIMUM SHEAR STRESS MAKE WITH ($\bar{1}10$) PLANE, RESPECTIVELY. THE SCHMID ANGLE FOR SLIP IN THE [001] DIRECTION IS λ_0. SIMILARLY FOR χ_1', ψ_1 AND λ_1 WITH RESPECT TO ($\bar{1}01$) PLANE AND [111] DIRECTION, χ_2', ψ_2 AND λ_2 WITH RESPECT TO (101) PLANE AND [$\bar{1}11$] DIRECTION.)

XBL 6911-5998

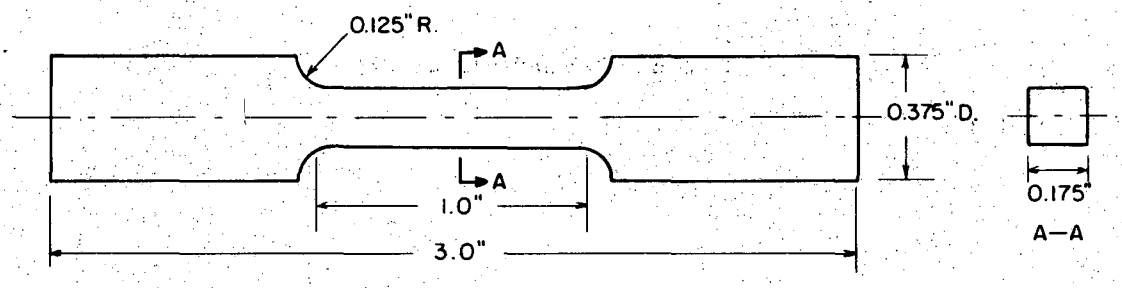

FIG. 2a TENSILE SPECIMEN

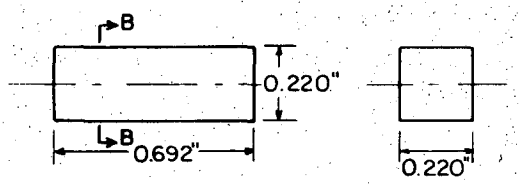

FIG. 2b COMPRESSIVE SPECIMEN

XBL 6910-5795

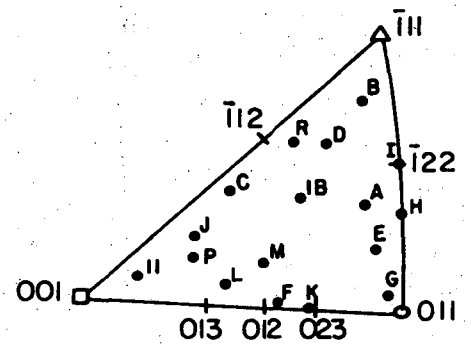

FIG. 3a ORIENTATIONS OF THE SPECIMENS.

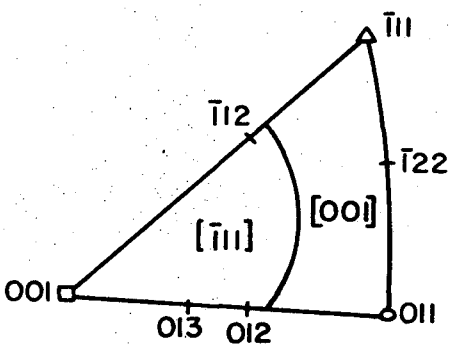

FIG. 3b ORIENTATION DEPENDENCE OF SLIP SYSTEM AT 237.5°K IN TENSION.

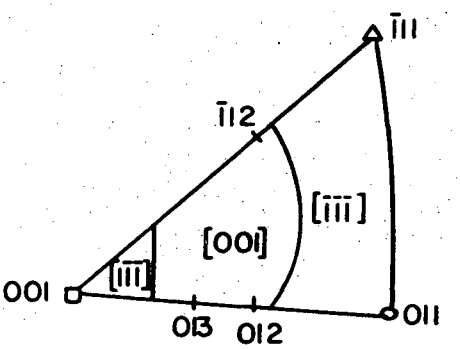

FIG. 3c ORIENTATION DEPENDENCE OF SLIP SYSTEM AT 237.5°K IN COMPRESSION.

XBL 6910-5796

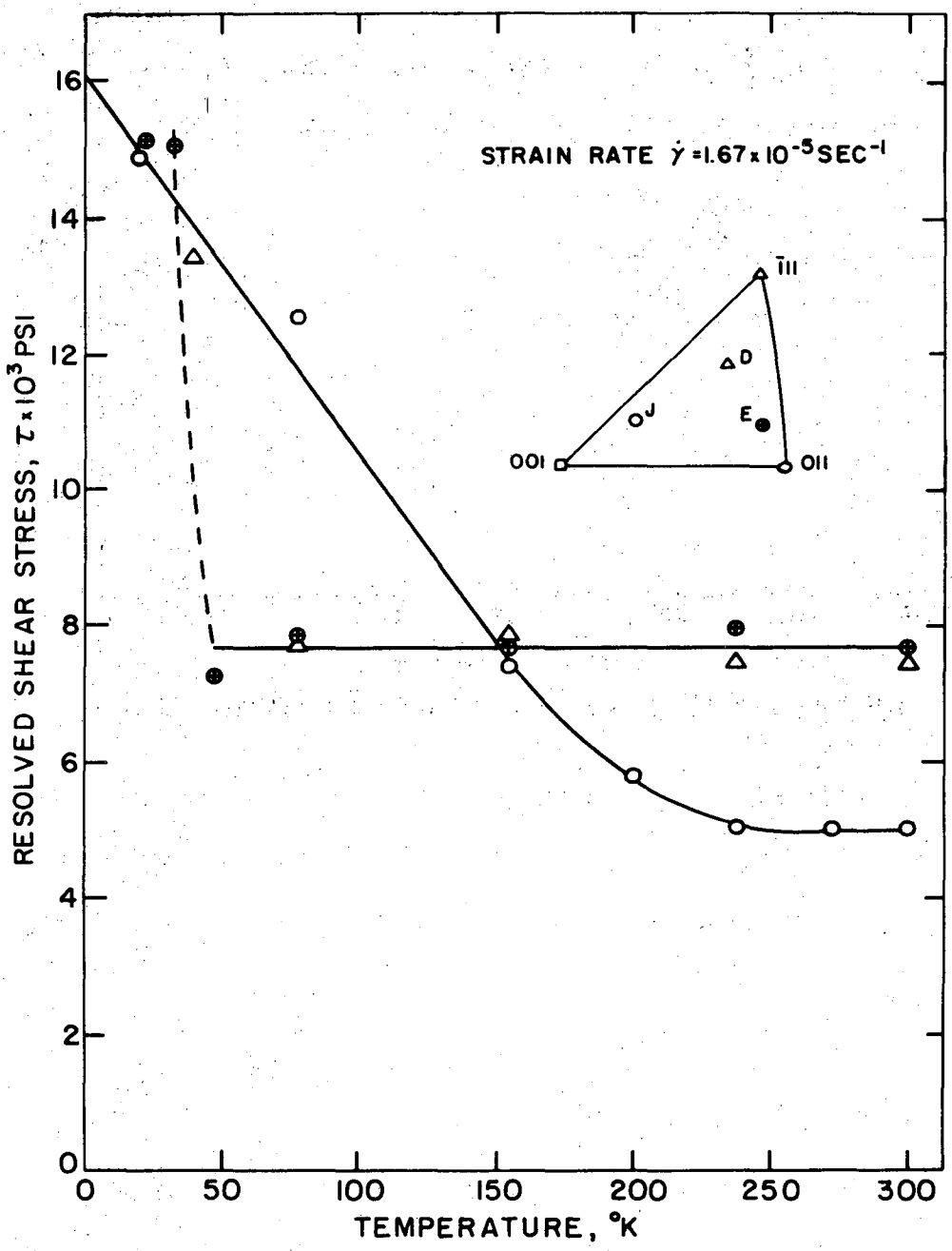

FIG. 4. RESOLVED SHEAR STRESS vs. TEMPERATURE.

XBL 6911-5996

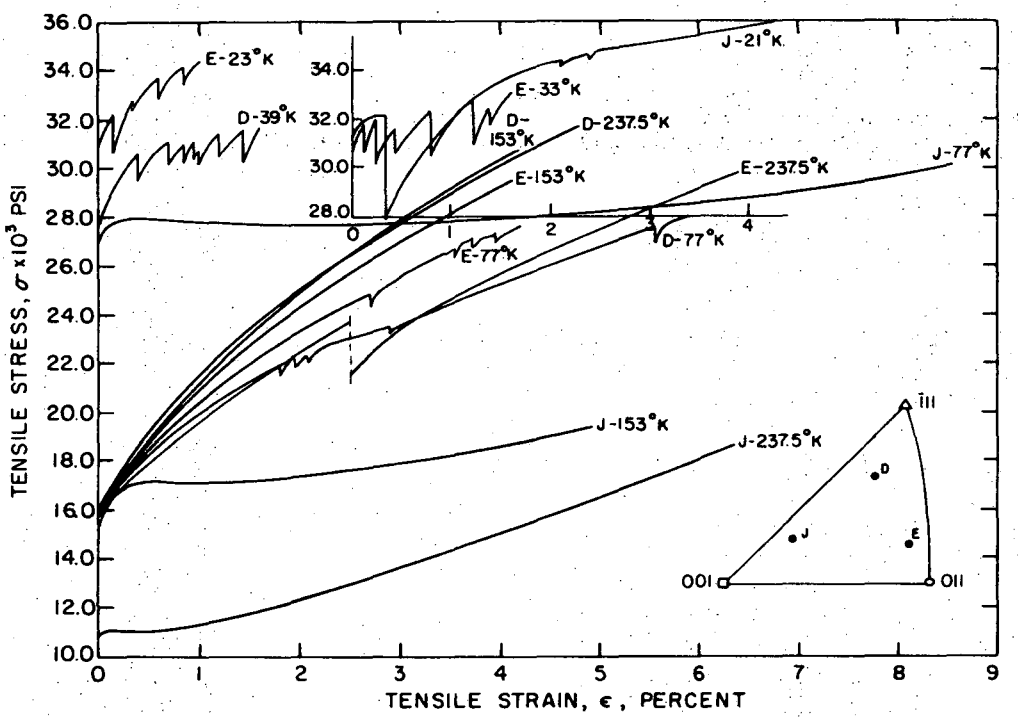

FIG. 5 STRESS vs. STRAIN CURVES FOR AgMg SINGLE CRYSTALS IN DIFFERENT ORIENTATIONS TESTED IN TENSION AT VARIOUS TEMPERATURES. ($\dot{\gamma} \simeq 1.67 \times 10^{-5}$/SEC.)

XBL 6910-5797

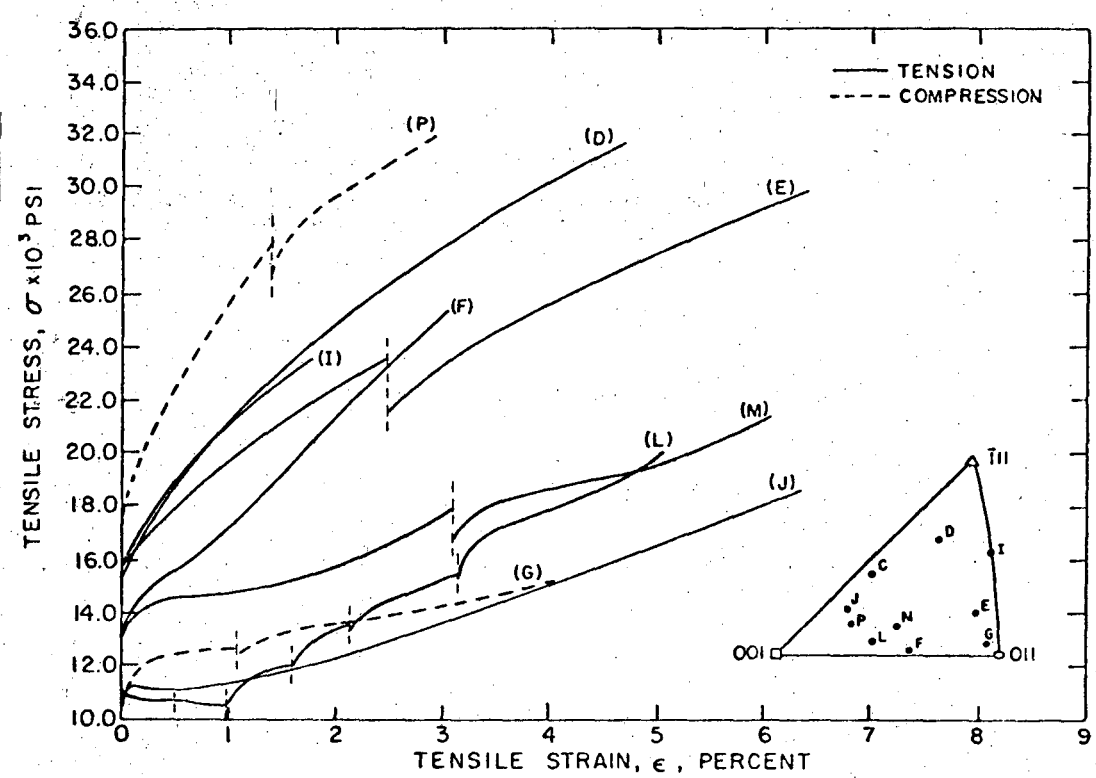

FIG. 6 STRESS vs. STRAIN CURVES FOR AgMg SINGLE CRYSTALS TESTED IN TENSION AND COMPRESSION. ($T = 237.5°K$; $\dot{\gamma} \simeq 1.67 \times 10^{-5}$/SEC.)

XBL 6910-5798

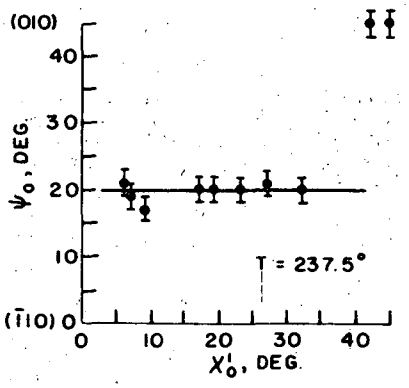

a. EFFECT OF ORIENTATION ON THE SLIP PLANE FOR CRYSTALS ORIENTED NEAR [1̄11]-[011] BOUNDARY TESTED IN TENSION.

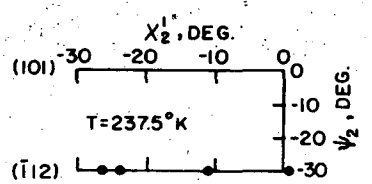

b. EFFECT OF ORIENTATION ON THE SLIP PLANE FOR CRYSTALS ORIENTED NEAR [011] DIRECTION TESTED IN TENSION.

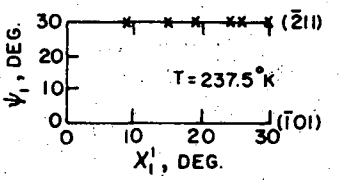

c. EFFECT OF ORIENTATION ON THE SLIP PLANE FOR CRYSTALS ORIENTED NEAR [1̄11]-[011] BOUNDARY TESTED IN COMPRESSION.

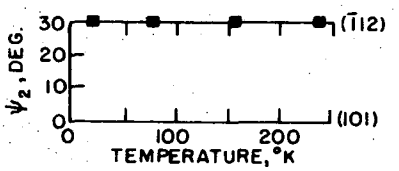

d. EFFECT OF TEMPERATURE ON THE SLIP PLANE FOR CRYSTALS IN ORIENTATION (J) TESTED IN TENSION.

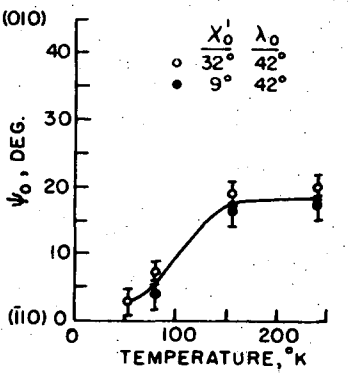

e. EFFECT OF TEMPERATURE ON THE SLIP PLANE FOR CRYSTALS IN ORIENTATIONS (E) AND (D) TESTED IN TENSION.

FIG. 7 THE SLIP GEOMETRY.
($\dot{\gamma} \approx 1.67 \times 10^{-5}$/SEC)

XBL 6910-5806

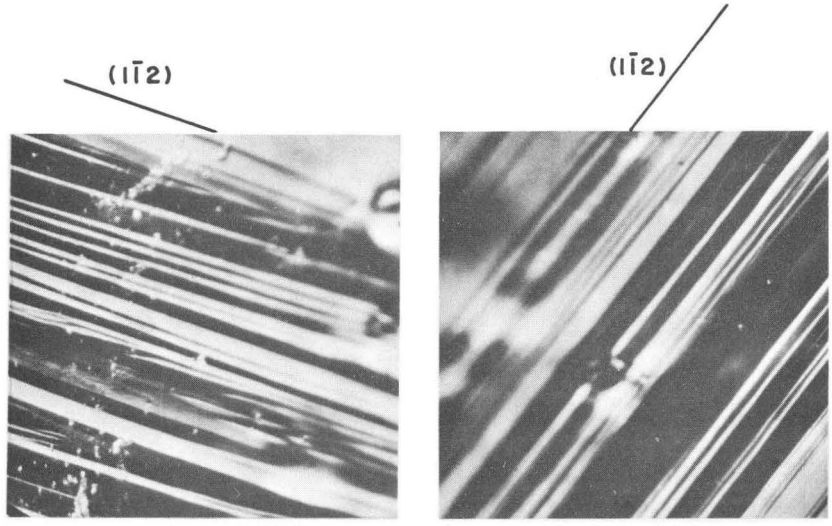

(a) FACE (b) SIDE

FIG. 8a SLIP TRACES OF SPECIMEN LI-19 DEFORMED AT 237.5°K TO 2.0% STRAIN IN TENSION "L."

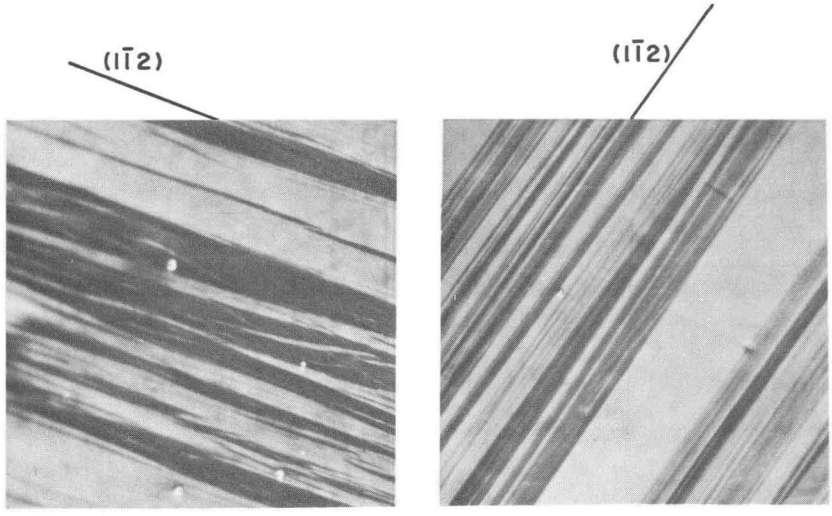

(a) FACE (b) SIDE

FIG. 8b SLIP TRACES OF SPECIMEN LI-19 DEFORMED AT 237.5°K TO 3.0% STRAIN IN TENSION "L."

XBB 6910-6591

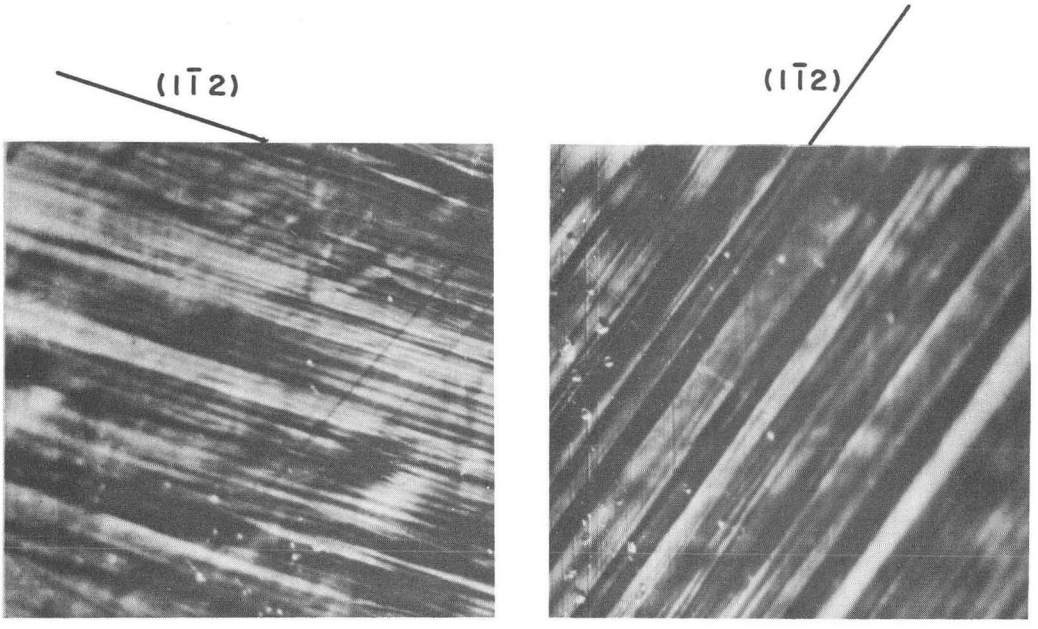

(a) FACE (b) SIDE

FIG. 8c SLIP TRACES OF SPECIMEN LI-19 DEFORMED AT 237.5 °K TO 5.0% STRAIN IN TENSION "L."

XBB 6910-6605

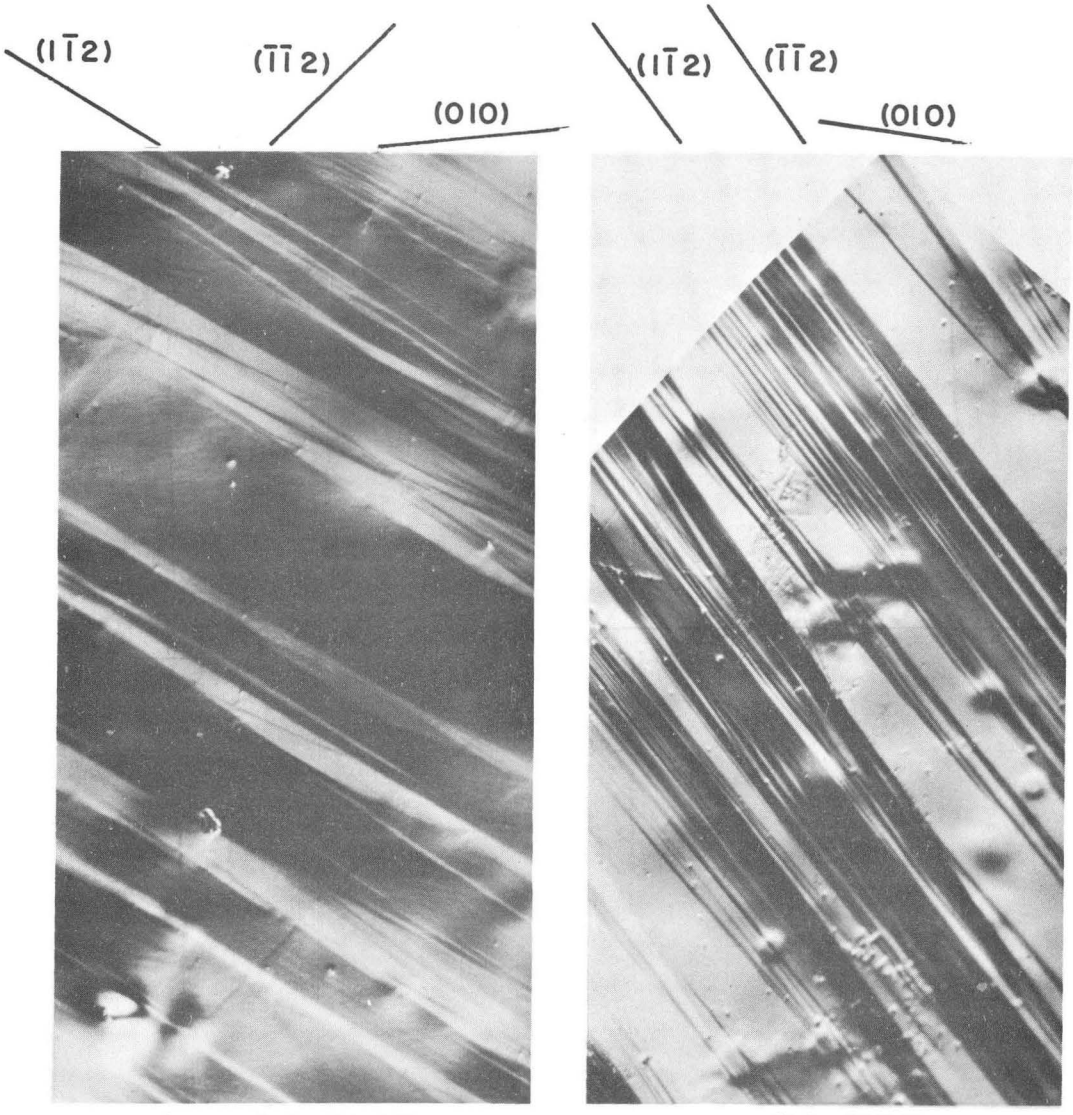

(a) FACE (b) SIDE

FIG. 8d SLIP TRACES OF SPECIMEN F2-19 DEFORMED AT 237.5°K TO 3.0% STRAIN IN TENSION "F."

XBB 6910-6600

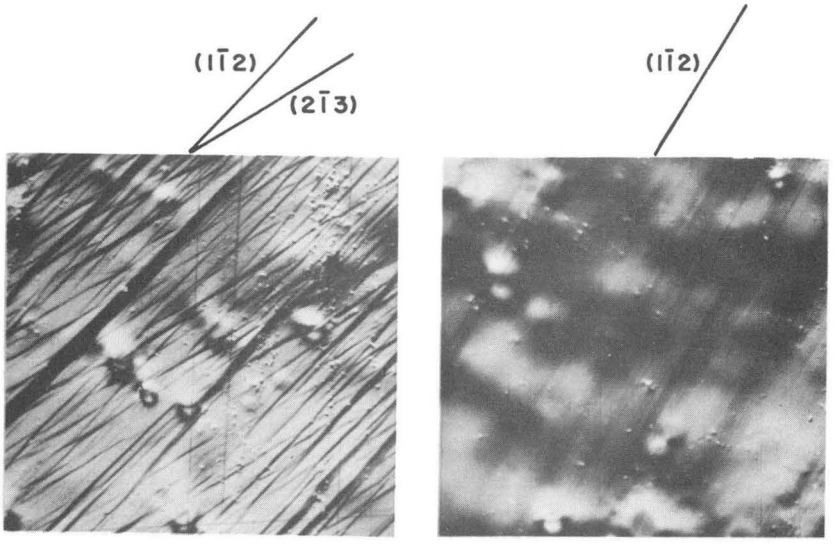

(a) FACE (b) SIDE

FIG. 8e SLIP TRACES OF SPECIMEN C1-19 DEFORMED AT 237.0°K TO 1.5% STRAIN IN TENSION "C."

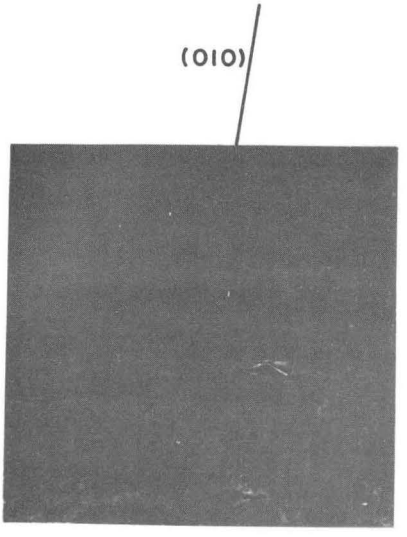

FIG. 8f SLIP TRACES OF SPECIMEN G1-19 DEFORMED AT 237.5°K TO 3.0% STRAIN IN TENSION "G."

XBB 6910-6589

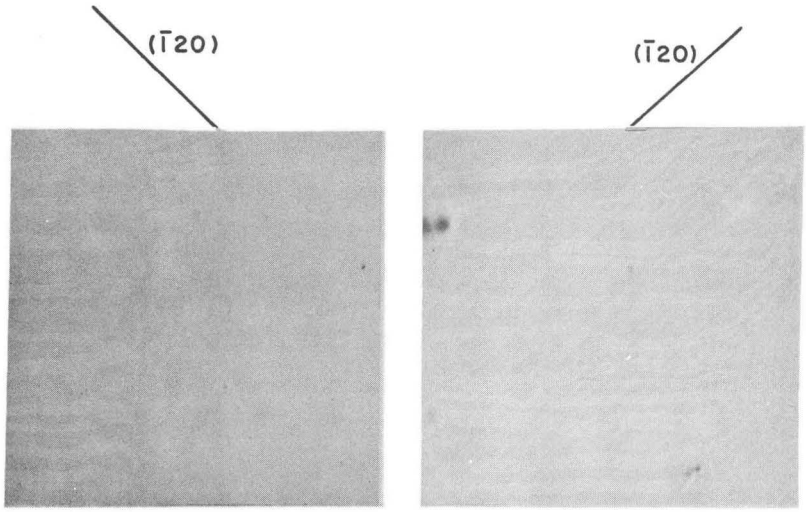

(b) SIDE (a) FACE

FIG. 8g SLIP TRACES OF SPECIMEN AI-21 DEFORMED AT 237.5°K TO 4.0% STRAIN IN TENSION "A."

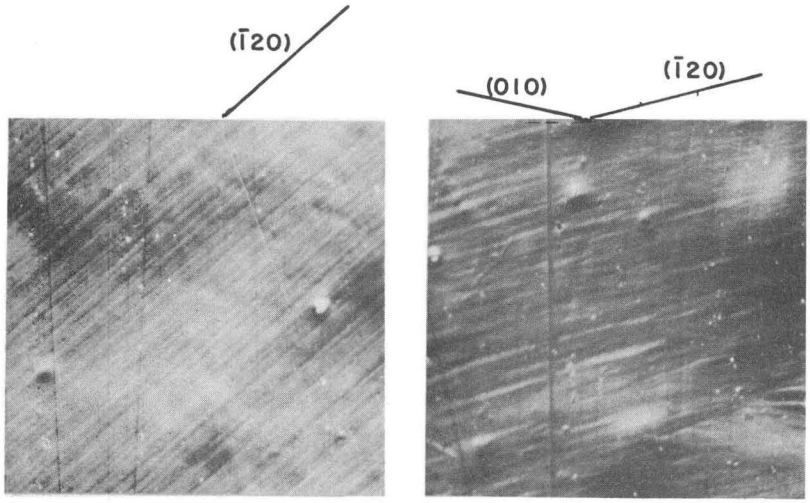

(b) SIDE (a) FACE

FIG. 8h SLIP TRACES OF SPECIMEN II-20 DEFORMED AT 237.5°K TO 4.0% STRAIN IN TENSION "I."

XBB 6910-6601

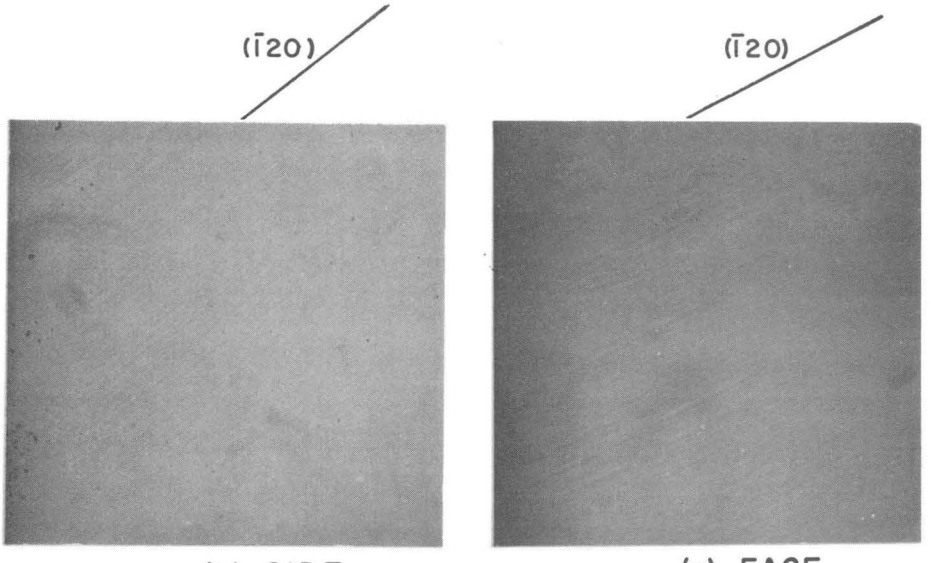

(b) SIDE (a) FACE

FIG. 8i SLIP TRACES OF SPECIMEN HI-21 DEFORMED AT 237.5 °K TO 4.0% STRAIN IN TENSION "H."

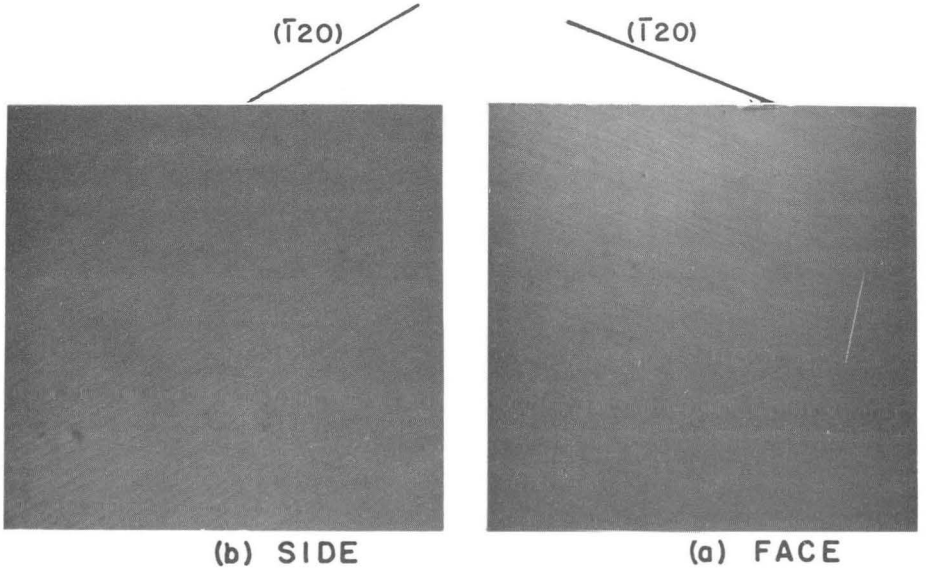

(b) SIDE (a) FACE

FIG. 8j SLIP TRACES OF SPECIMEN BI-21 DEFORMED AT 237.5°K TO 4.0% STRAIN IN TENSION "B."

XBB 6910-6598

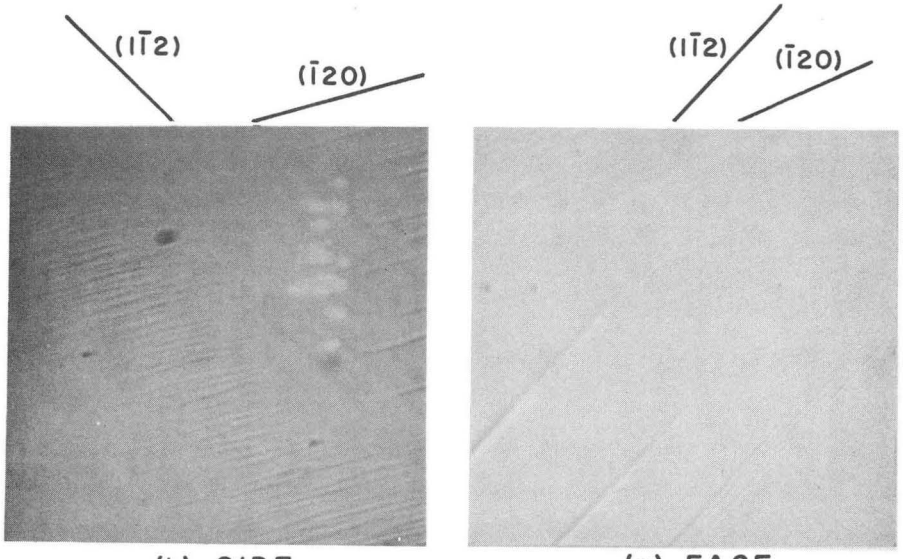

(b) SIDE (a) FACE

FIG. 8k SLIP TRACES OF SPECIMEN R1-21 DEFORMED AT 237.5°K TO 2.0% STRAIN IN TENSION "R."

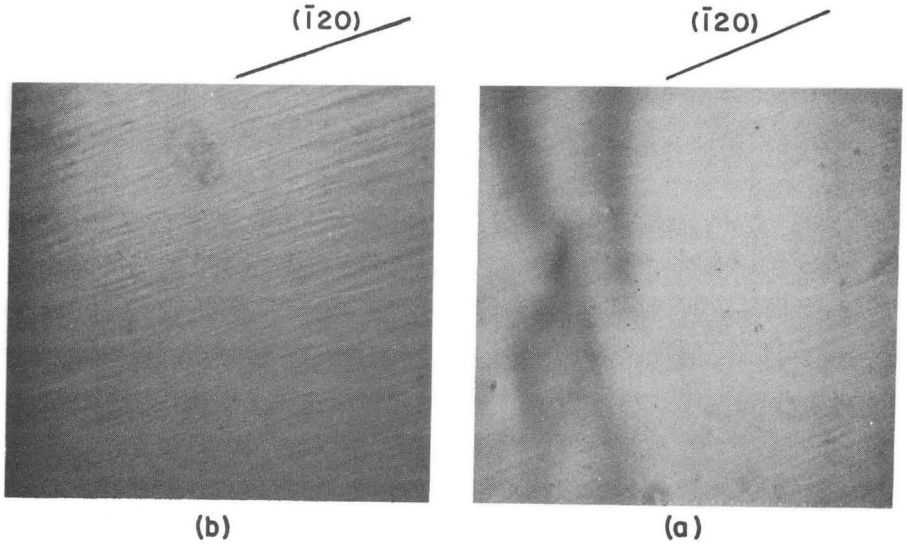

(b) (a)

FIG. 8l SLIP TRACES OF SPECIMEN R1-21 DEFORMED AT 237.5°K TO 6.0% STRAIN IN TENSION "R."

XBB 6910-6604

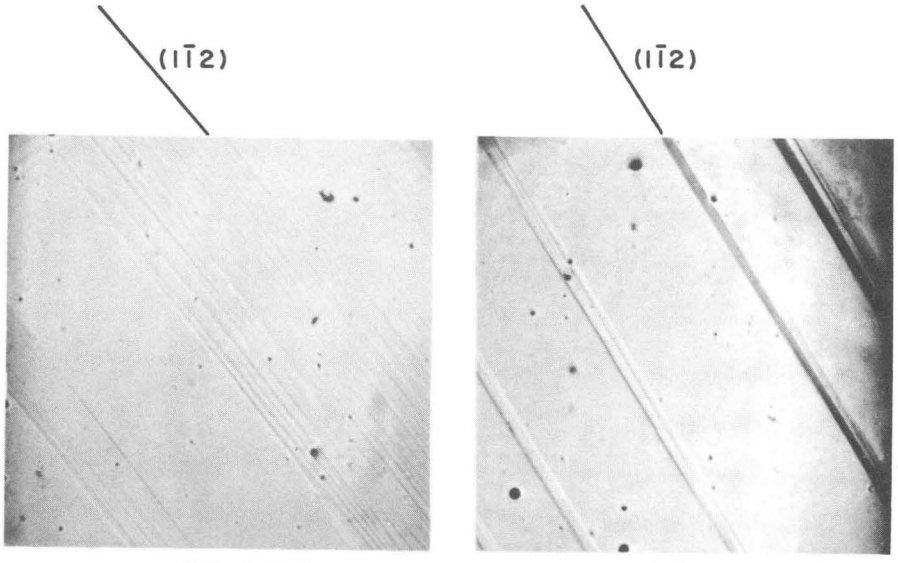

(b) SIDE (a) FACE

FIG. 8m SLIP TRACES OF SPECIMEN IB-21 DEFORMED AT 237.5°K TO 2.0% STRAIN IN TENSION "IB."

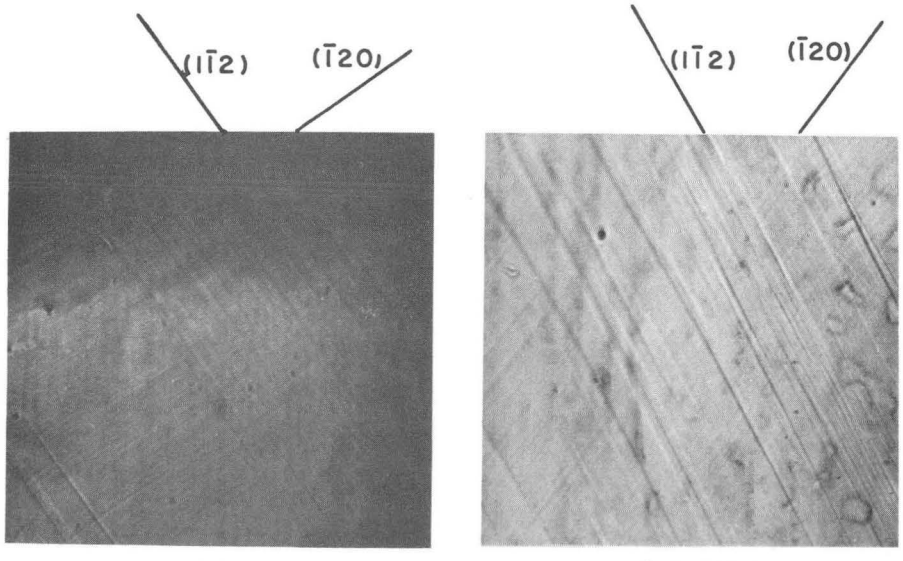

(b) SIDE (a) FACE

FIG. 8n SLIP TRACES OF SPECIMEN IB-21 DEFORMED AT 237.5°K TO 6.0% STRAIN IN TENSION "IB."

XBB 6910-6595

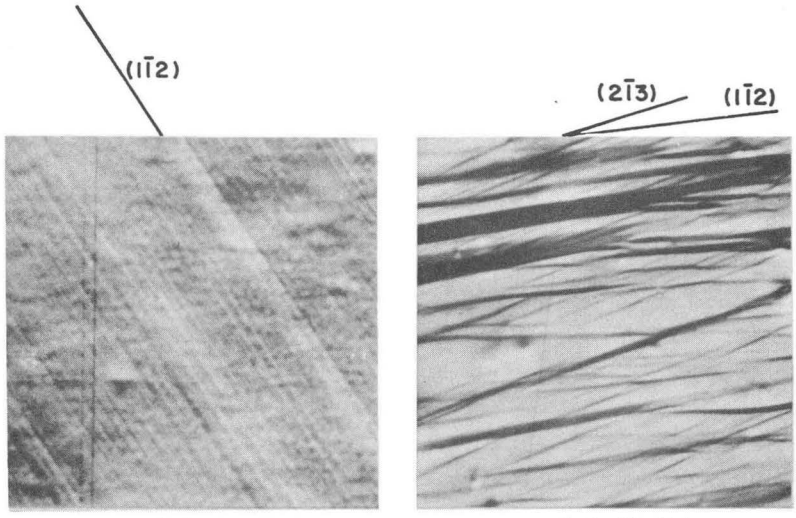

(b) SIDE (a) FACE

FIG. 9a SLIP TRACES OF SPECIMEN J2-19 DEFORMED AT 153°K TO 5.0% STRAIN IN TENSION "J."

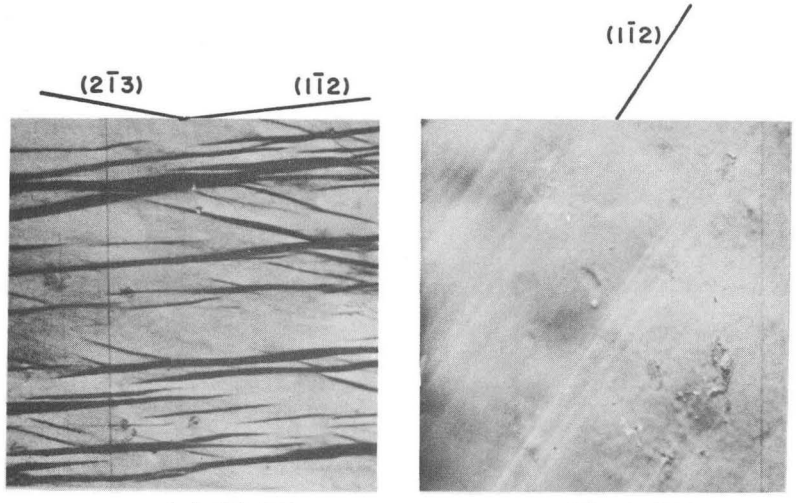

(a) FACE (b) SIDE

FIG. 9b SLIP TRACES OF SPECIMEN J1-19 DEFORMED AT 237.5°K TO 6.5% STRAIN IN TENSION "J."

XBB 6910-6594

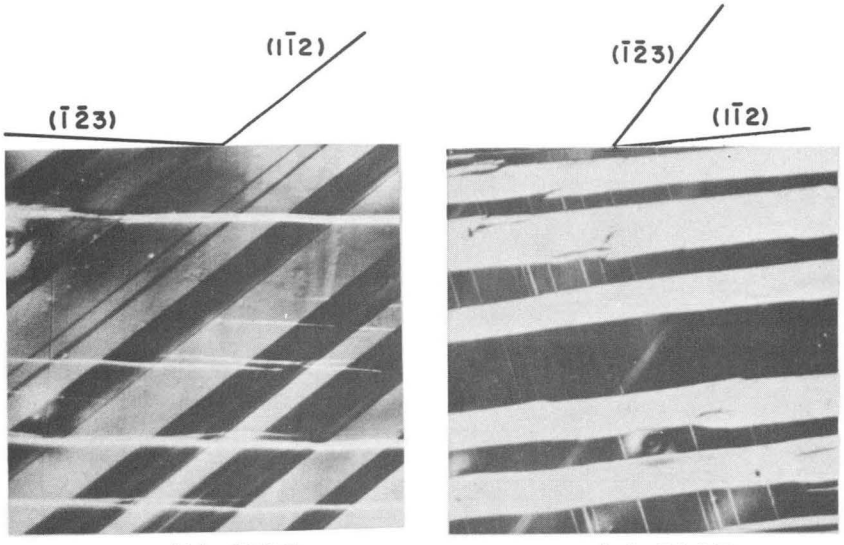

(b) SIDE (a) FACE

FIG. 9c SLIP TRACES OF SPECIMEN J4-19 DEFORMED AT 21°K TO 4.5% STRAIN IN TENSION "J."

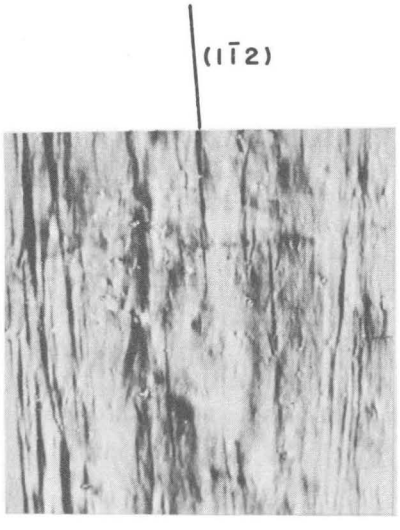

FIG. 9d SLIP TRACES OF SPECIMEN J3-19 DEFORMED AT 77°K TO 8.5% STRAIN IN TENSION "J."

XBB 6910-6593

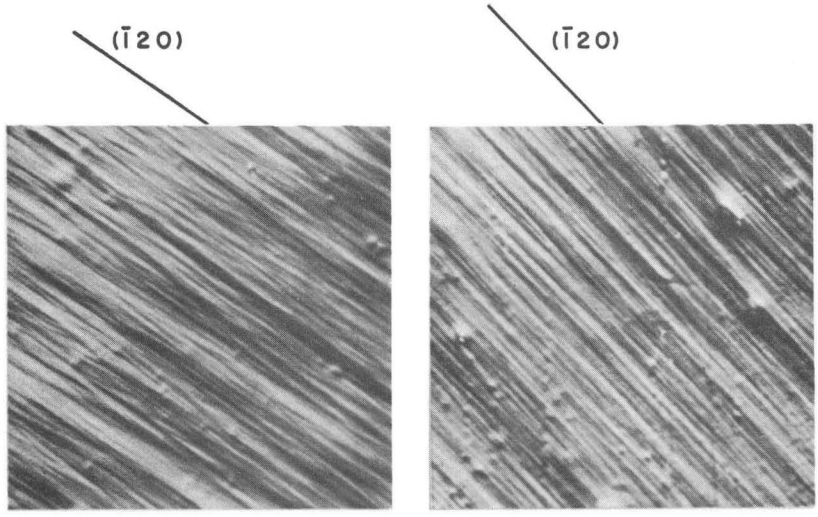

(a) FACE (b) SIDE

FIG. 10 a SLIP TRACES OF SPECIMEN D1-20 DEFORMED AT 237.5°K TO 4.50% STRAIN IN TENSION "D."

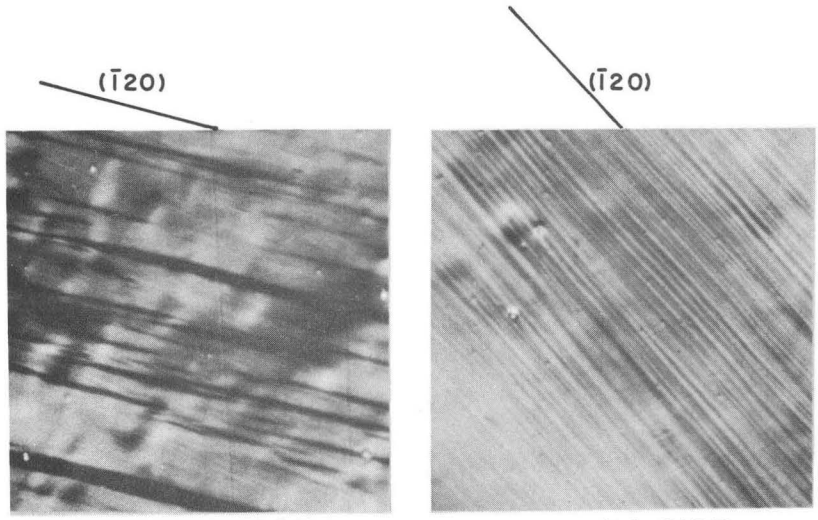

(a) FACE (b) SIDE

FIG. 10 b SLIP TRACES OF SPECIMEN D2-20 DEFORMED AT 153°K TO 4.25% STRAIN IN TENSION "D."

XBB 6910-6597

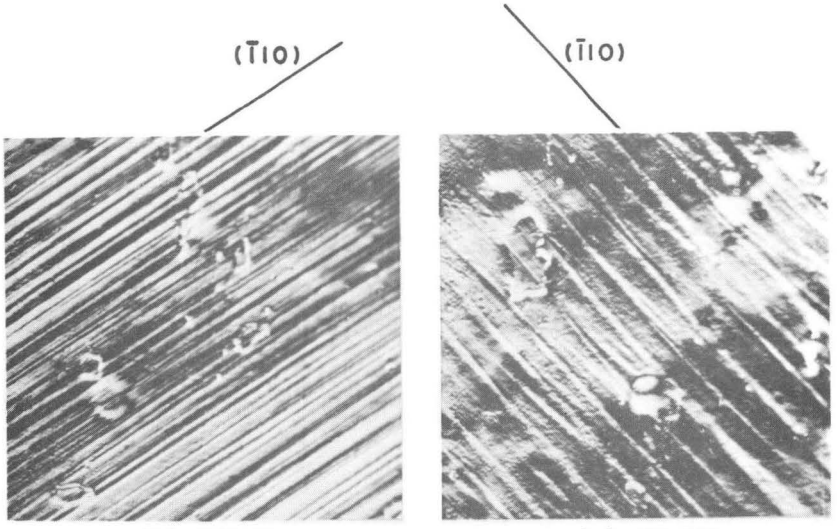

(b) SIDE (a) FACE

FIG. 10c SLIP TRACES OF SPECIMEN D3-20 DEFORMED AT 77°K TO 6.0% STRAIN IN TENSION "D."

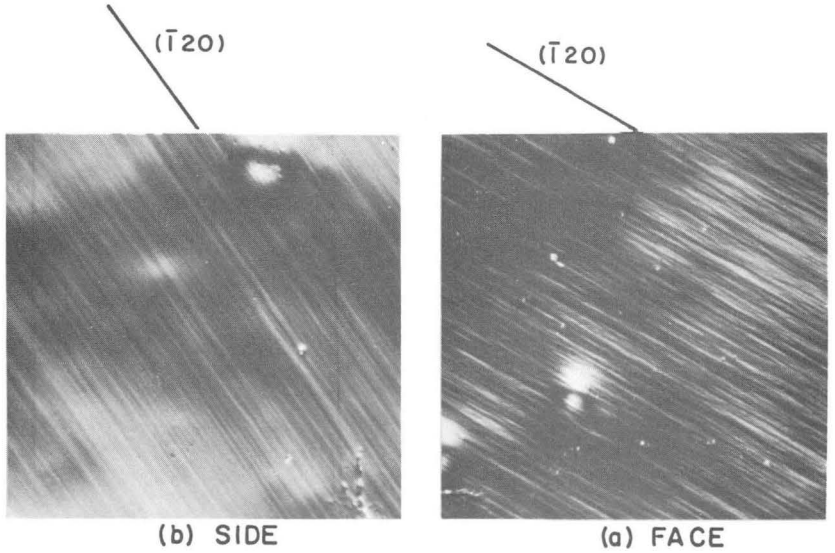

(b) SIDE (a) FACE

FIG. 11a SLIP TRACES OF SPECIMEN E1-20 DEFORMED AT 237.5°K TO 7.0% STRAIN IN TENSION "E."

XBB 6910-6602

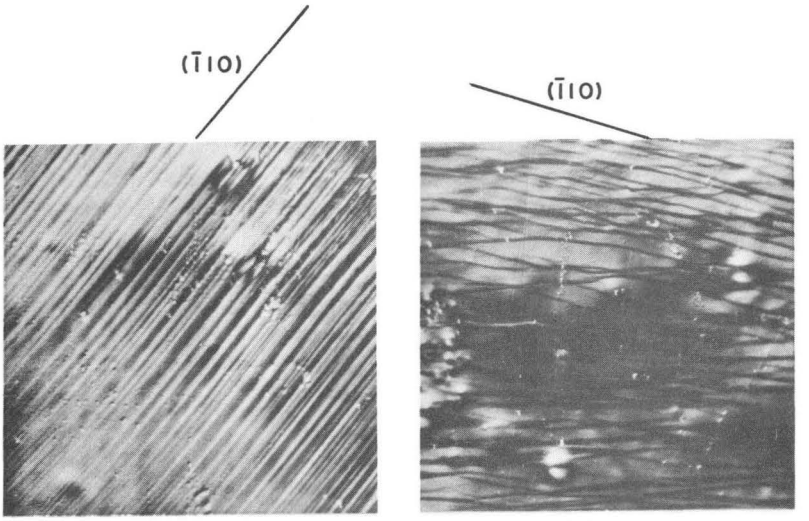

(b) SIDE (a) FACE

FIG. 11b SLIP TRACES OF SPECIMEN E3-20 DEFORMED AT 77°K TO 4.25% STRAIN IN TENSION "E."

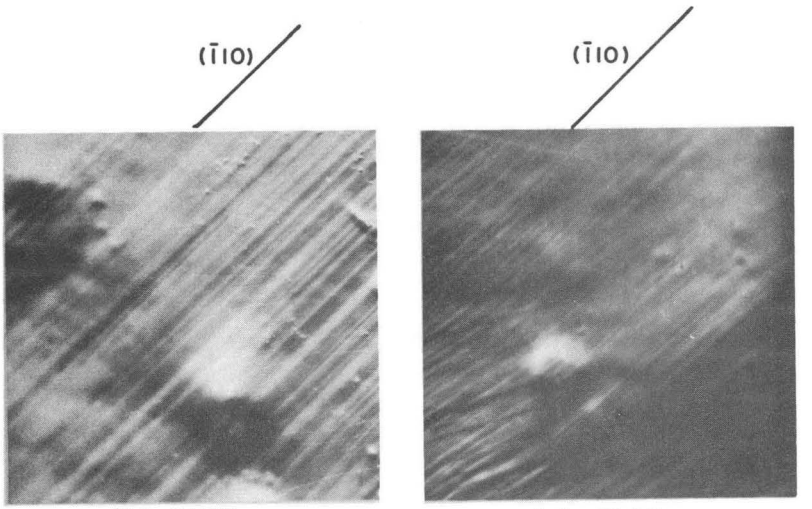

(b) SIDE (a) FACE

FIG. 11c SLIP TRACES OF SPECIMEN E4-20 DEFORMED AT 48°K TO 5.0% STRAIN IN TENSION "E."

XBB 6910-6603

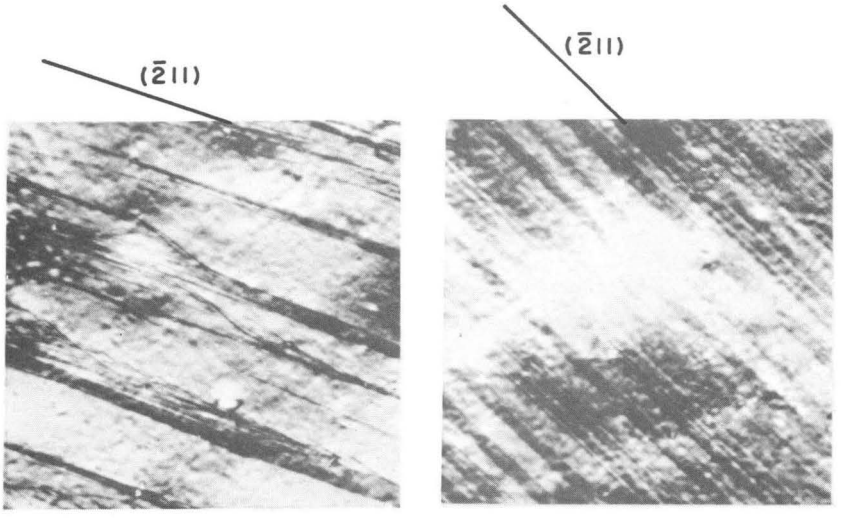

(a) FACE (b) SIDE

FIG. 11d SLIP TRACES OF SPECIMEN E5-20 DEFORMED AT 33°K TO 1.5% STRAIN IN TENSION "E."

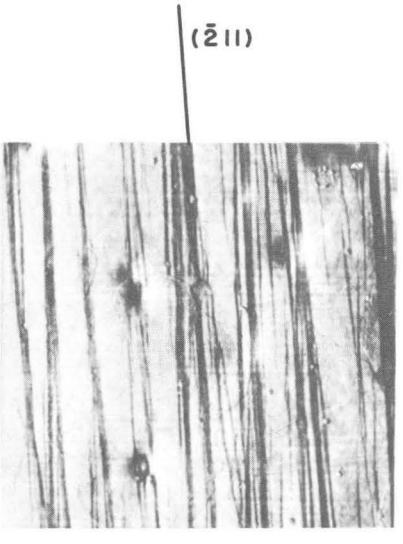

FIG. 11e SLIP TRACES OF SPECIMEN E6-20 DEFORMED AT 23 °K TO 1.0% STRAIN IN TENSION "E."

XBB 6910-6596

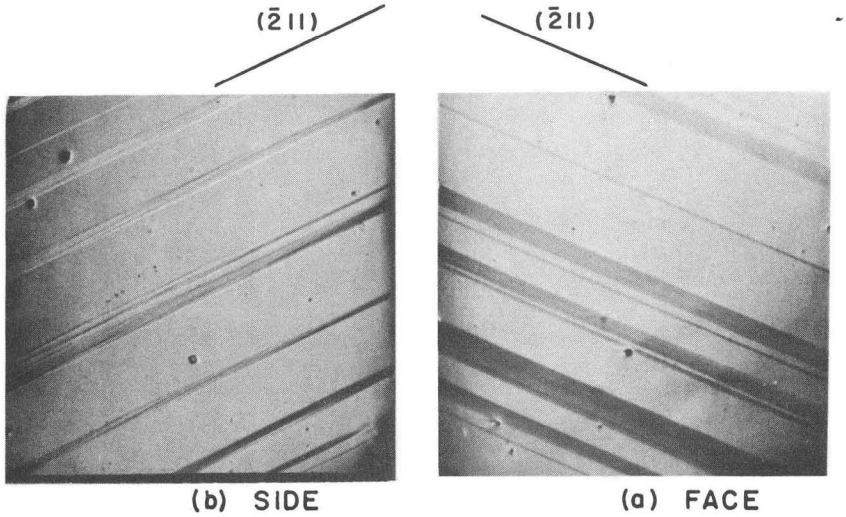

(b) SIDE (a) FACE

FIG. 12 a SLIP TRACES OF SPECIMEN R1-21 DEFORMED AT 237.5 °K IN COMPRESSION "R."

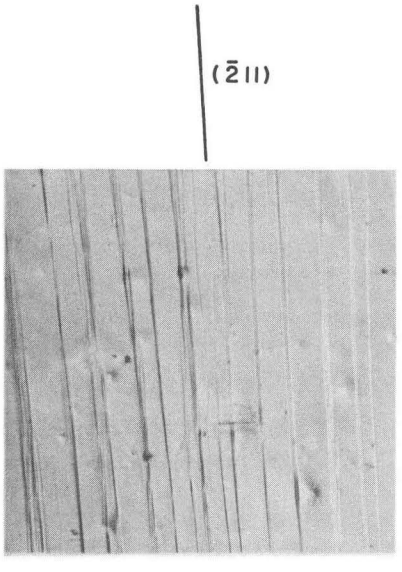

FIG. 12 b SLIP TRACES OF SPECIMEN H1-21 DEFORMED AT 237.5 °K IN COMPRESSION "H."

XBB 6910-6590

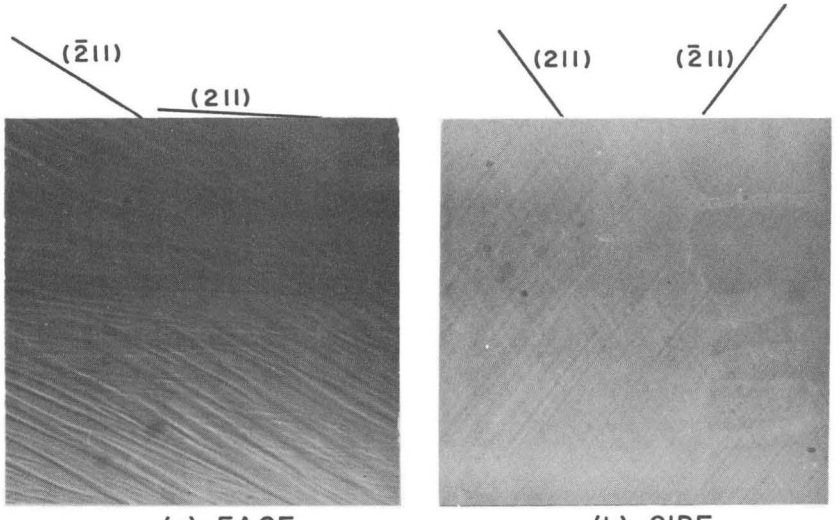

(a) FACE (b) SIDE

FIG. 12c SLIP TRACES OF SPECIMEN K1-21 DEFORMED AT 237.5°K IN COMPRESSION "K".

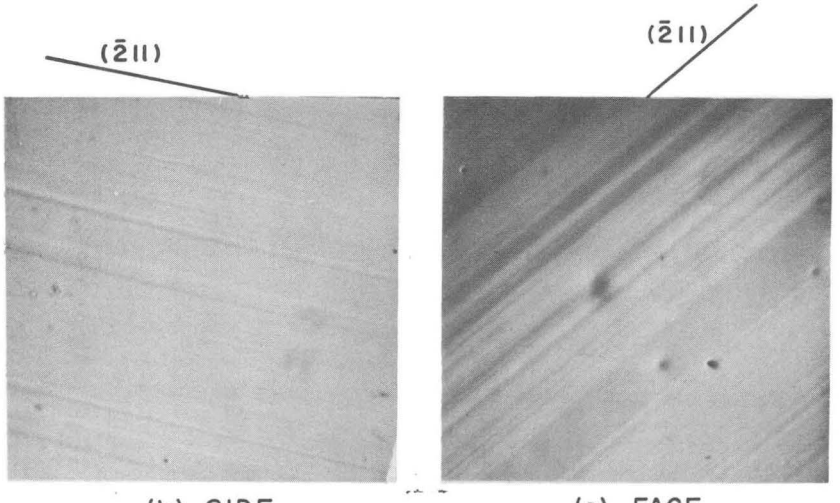

(b) SIDE (a) FACE

FIG. 12d SLIP TRACES OF SPECIMEN A1-21 DEFORMED AT 237.5°K IN COMPRESSION "A".

XBB 6910-6592

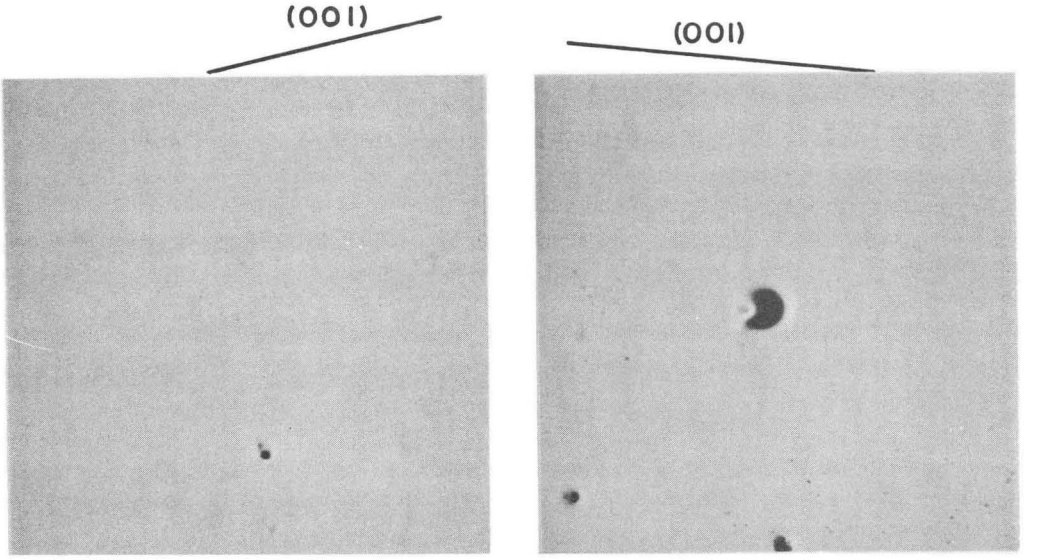

(b) SIDE (a) FACE

FIG. 12e SLIP TRACES OF SPECIMEN P1-21 DEFORMED AT 237.5°K TO 1.40 % STRAIN IN COMPRESSION "P."

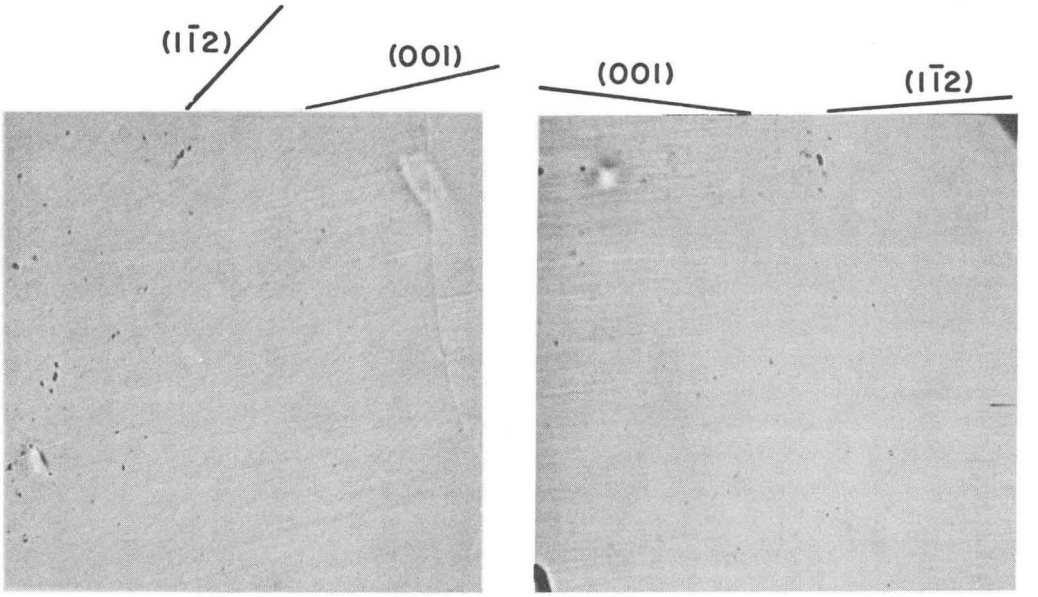

(b) SIDE (a) FACE

FIG. 12f SLIP TRACES OF SPECIMEN P1-21 DEFORMED AT 237.5°K TO 3.0 % STRAIN IN COMPRESSION "P."

XBB 6910-6599

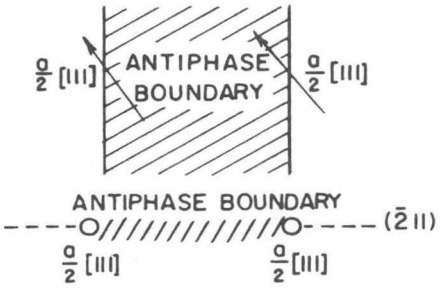

FIG. 13a $\frac{a}{2}$[111] TYPE SUPERLATTICE DISLOCATION IN B_2 (BCC) TYPE SUPERLATTICE.

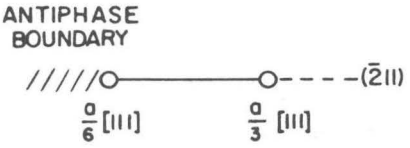

FIG. 13b POSSIBLE SPLITTING OF THE CORE OF $\frac{a}{2}$[111] EDGE DISLOCATION.

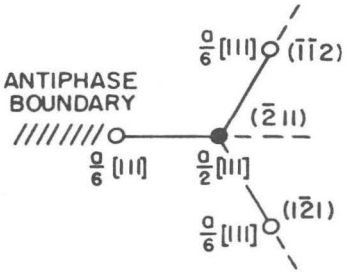

FIG. 13c POSSIBLE SPLITTING OF THE CORE OF $\frac{a}{2}$[111] SCREW DISLOCATION.

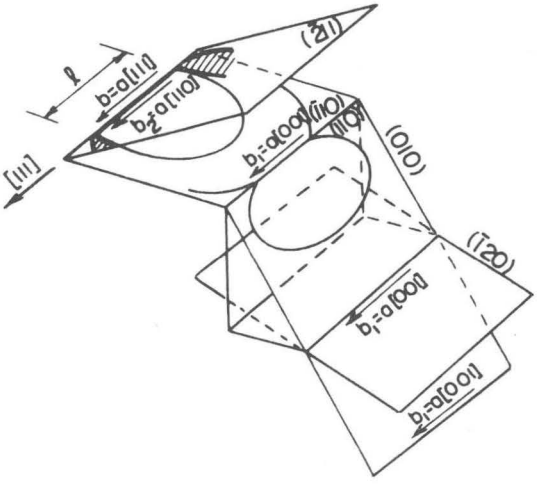

FIG. 13d RECOMBINATION OF $\frac{a}{2}$[111] PARTIALS INTO PERFECT a[111] SCREW DISLOCATION ALONG LENGTH ℓ. BOWING OUT OF a[001] SCREW DISLOCATION AND CONTINUOUS CROSS SLIP ON {110} AND {100} PLANES TO PRODUCE MACROSCOPIC SLIP ON PLANES OF THE [001] ZONE AFTER SPLITTING OF a[111] INTO a[001] AND a[110] SCREW DISLOCATIONS.

XBL 6910-5804

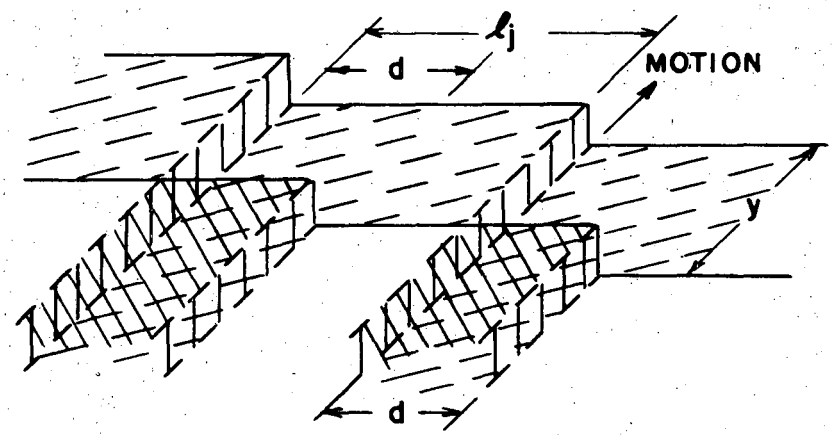

FIG. 14. FORMATION OF ANTIPHASE BOUNDARY TUBES BY MOTION OF JOGGED SUPERDISLOCATIONS.

XBL 6911-5997

LEGAL NOTICE

This report was prepared as an account of Government sponsored work. Neither the United States, nor the Commission, nor any person acting on behalf of the Commission:

A. Makes any warranty or representation, expressed or implied, with respect to the accuracy, completeness, or usefulness of the information contained in this report, or that the use of any information, apparatus, method, or process disclosed in this report may not infringe privately owned rights; or

B. Assumes any liabilities with respect to the use of, or for damages resulting from the use of any information, apparatus, method, or process disclosed in this report.

As used in the above, "person acting on behalf of the Commission" includes any employee or contractor of the Commission, or employee of such contractor, to the extent that such employee or contractor of the Commission, or employee of such contractor prepares, disseminates, or provides access to, any information pursuant to his employment or contract with the Commission, or his employment with such contractor.

TECHNICAL INFORMATION DIVISION
LAWRENCE RADIATION LABORATORY
UNIVERSITY OF CALIFORNIA
BERKELEY, CALIFORNIA 94720